Transverse Single Spin Asymmetry in J/ψ Production in Run15 Polarized $p+p$, $p+$Al and $p+$Au Collision at $\sqrt{s}=200$GeV

Chen Xu, Jin Huang, Haiwang Yu, Stephen Pate, vassilios papavassiliou, Xiaorong Wang

June 27, 2017

Abstract

The transverse single spin asymmetry of high p_T muons from J/ψ production in polarized $p+p$ and $p+$Au collisions at $\sqrt{s}=200$ GeV has been measured from Run15 data. The Run15 pp data recorded luminosity is 50 pb^{-1} with average beam polarization about 55% and the recorded luminosity of $1.27pb^{-1}$ with average beam polarization about 60% for pAu data which is given by Run summery from CAD.

1 Run selection

1.1 Run selection with pp data

Following runs are excluded:

• Remove runs due to the missing of Spin patterns and GL1p scalar in Spin Database:
424877 425011 425403 425747 425763 427129 427136 427137 428265 428607 428717 429503 429590 430607 431026 431932

• Remove runs due to abnormal GL1p scalar in Spin Database:
426308 426353 431831 431832 431833 431834 431835 431837 431840 431845 431846 431859 431860 431886 431888

• Remove the runs due to Zero BBCin count in Spin Database:
426313 426315 426316 426319 426320 431854

• Remove the runs due to high number of dead packets or dimuon yield per minimum bias events is too low or too high:
427670 427671 427672 427673 427674 427708 427710 427711 427712 427713 427805 427806 427807 427811 427813 427814 427815 427829 427878 427879 427881 427882 427885 427886 427887 427964 430402 430519 427656 425423 429886 429887 430402 430519 427656

• Remove runs due to increasing polarization in same fill:
424227

• Remove runs due to no diumuon events after cut:

424439

• Remove runs due to the short duration (less than about 10 mins):
422074 422084 422319 422531 422562 422640 423041 423311 423546 423549 423576 424443 424627 424759 424886 425168 425290 425583 425688 426443 427129 427136 427264 427362 427366 427377 427657 427658 427673 427709 427810 427883 427968 427979 428211 428255 428260 428264 428266 428318 428323 428324 428451 428601 428728 428730 428733 428737 428754 428758 428892 429022 429024 429127 429365 429595 429678 429680 429696 429798 429888 430119 430121 430136 430137 430239 430494 430522 430563 430594 430600 430905 430906 431125 431137 431437 431608 431609 431836 431839 431844 431894

1.2 Run selection with pAu data

Following runs are excluded:
• Remove runs due to the missing of Spin patterns and GL1p scalar in Spin Database:
432641 433266 434147 434148 434150 434151 434699 434909 434982 434983 435939 434980 434981 434984
• Remove runs due to abnormal GL1p scalar in Spin Database:
435361
• Remove runs due to increasing polarization in same fill:
434360 434362 434363 434364 435525 435526 435527 435528 435529 435530 435601 435606 435826 435828 435832 435836 435841

1.3 Run selection with pAl data

Following runs are excluded:
• Remove runs due to abnormal GL1p scalar in Spin Database:
437101 437714 438033 438153
• Remove the runs due to high number of dead packets or dimuon yield per minimum bias events is too low or too high:
South Arm: 437353 437356 437358 437361 437362 437417 437421 437430 437431 437433 437434 437435 437440 437474 437478 437483 437484 437486 437487 437488 437568 437569 437572 437573 437574 437575 437583 437649 437650 437658 437659
North Arm: 437433

2 Event and track selection

Analysis cuts are placed on a track by track basis. The same cuts are applied for both pp, pAl and pAu case. The details for those cuts are shown as following:

• Kinematic Cut for dimuon: $0.42GeV < p_T < 10GeV$, $p_z < 100GeV$, $charge = 0$, Forward and backward pseudo-rapidity ($1.2 < |y| < 2.2$).

• Track Quality Cut for single muon: $DG0 < 25cm(N)$, $DG0 < 30cm(S)$, $DDG0 < 10$, $ntrhits > 9$, $nidhits > 5$, $lastgap > 2$, MuTr $DCA_r < 10$.

• Track Quality Cut for dimuon: $BBCz{-}vertex: -30 < z < 30cm$, $Evt\_vtxchi2 < 5$.

• Trigger Selection: 2D LL1 trigger and SG3&MUIDLL1($1D \parallel 1H$) trigger

A $p_T < 0.42GeV$ low side cut is applied considering the resolution of forward muon arms. The resolution is got from PYTHIA6 simulation where the difference between input and output p_x and p_y distributions are plotted and shown in figure 1. This cut will just cut off less than 1% dimuons as we can see in the p_T distribution plots in figure 2.

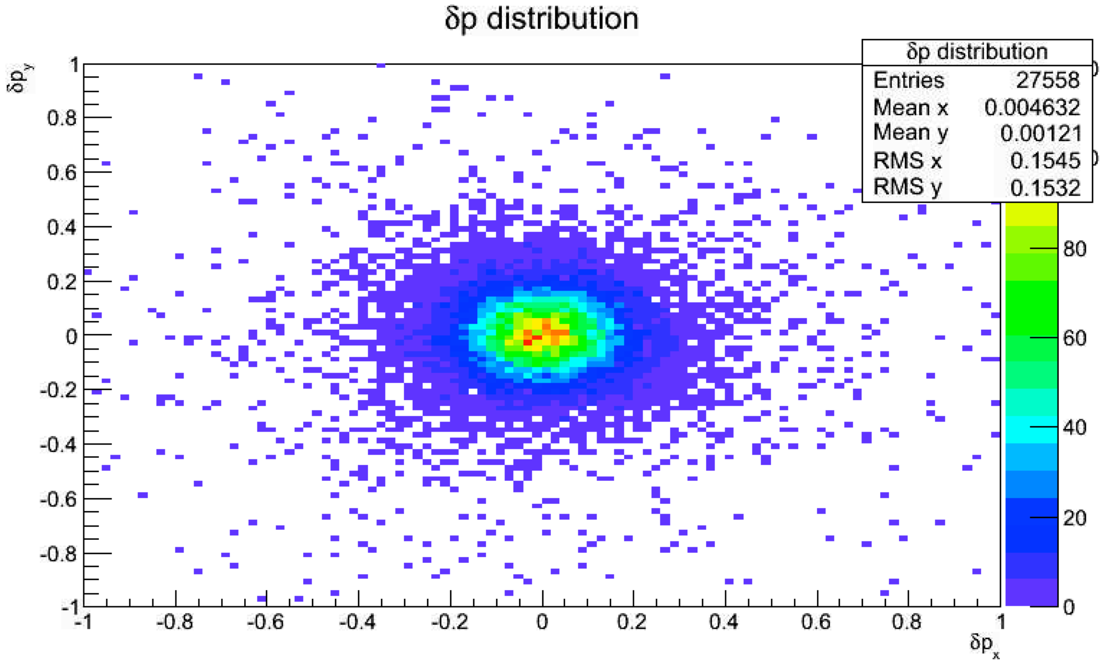

Figure 1: δp_x and δp_y are got by finding the difference between input and output p_x, p_y in PYTHIA6 simulation. A 2-σ cut ($\tilde{0}.3$ GeV) is made.

3 Background Fraction

Gaussian Process Regression(GPR) method is used to fit the background shapes without supposing a prior functional form. More details about GPR method can be found in Analysis Note AN1145.

The GPR method is trained on the data points in the 1.5-2.2 GeV and 4.3-6.0 GeV mass ranges in order to exclude the J/ψ and ψ' contributions to the mass spectrum and include only the data points that should correspond to background for the analysis.

For J/ψ invariant mass fit, the background which is got from GPR is extracted

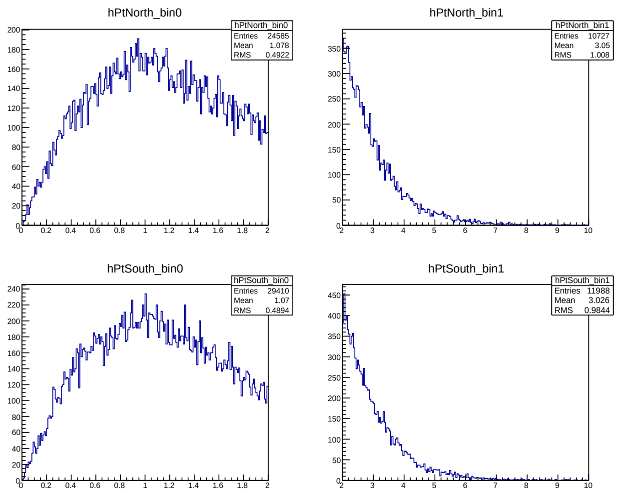

Figure 2: p_T distribution for North arm(top) and South arm(bottom) in pp data.

from real data point. Then J/ψ is fitted with Crystal Ball function while ψ' is fitted with a Gaussian function.

The Crystal Ball function is a gaussian which has been joined smoothly with a power law on one side such that it and the first and second derivative are continuous functions as defined in equation 11 in AN1178.

In this analysis, we fit dimuon invariant mass in three different p_T bins for both North and South arm which are $p_T \in (0-10)$ GeV, $p_T \in (0-2)$GeV, $p_T \in (2-10)$GeV for pp, pAl and pAu data. At the same time, two x_F bins were picked by making the statistic of each x_F bin in 2-σ J/ψ mass window equal. The x_F binning for pp, pAl and pAu data is $x_F \in (0.05-0.11)$ and $x_F \in (0.11-0.30)$. The background fraction is calculated within 2-σ J/ψ mass window.

Figure 3 to 7 show the GPR fitting for pp data, figure 8 to 12 show the GPR fitting for pAu data and figure 13 to 17 show the GPR fitting for pAl data.

Table 1 shows the background fraction in p_T bins from GPR for pp data
Table 2 shows the background fraction in p_T bins from GPR for pAu data
Table 3 shows the background fraction in p_T bins from GPR for pAl data
Table 4 shows the background fraction in x_F bins from GPR for pp data
Table 5 shows the background fraction in x_F bins from GPR for pAu data
Table 6 shows the background fraction in x_F bins from GPR for pAl data

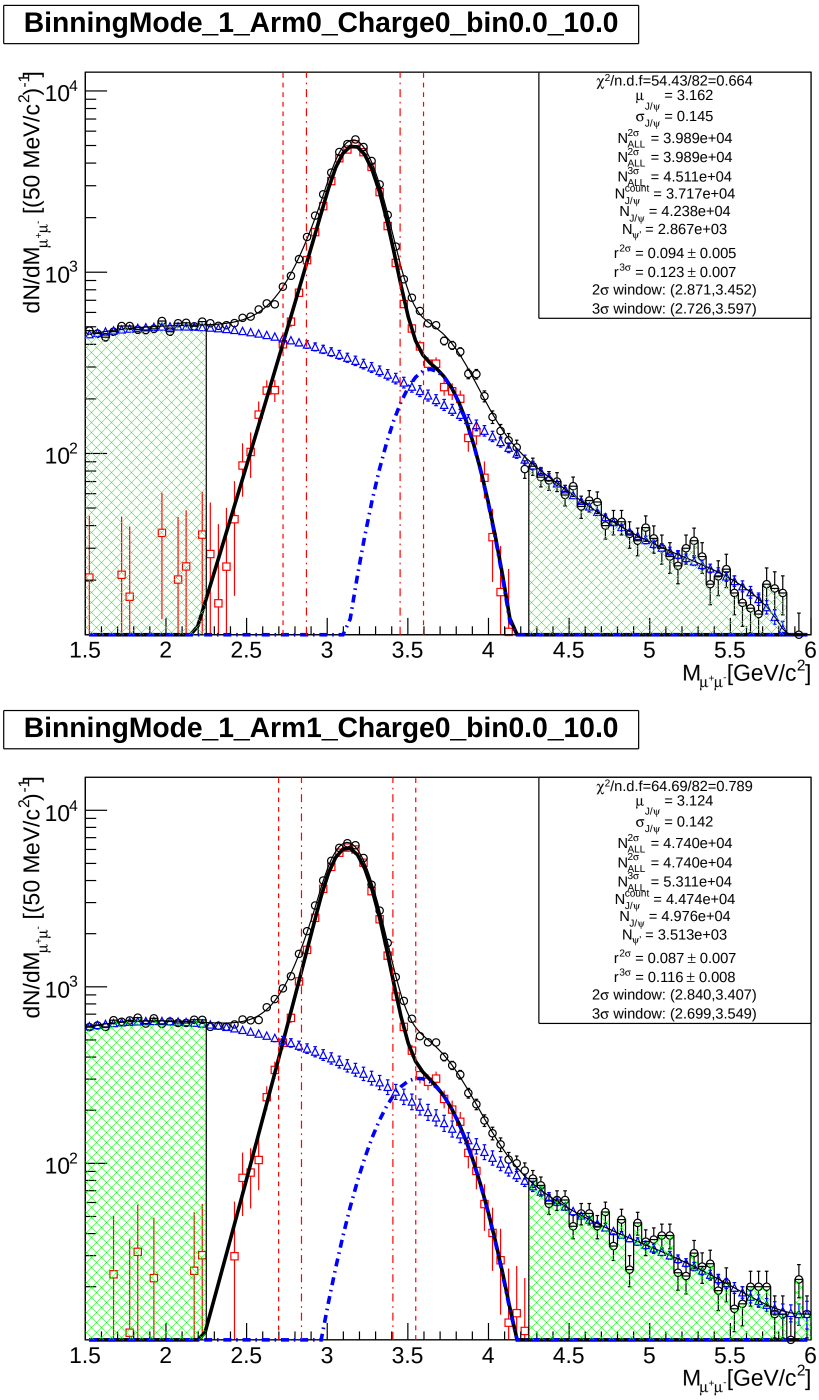

Figure 3: MuTr mass spectrum fits with GPR background estimation for $p_T = 0 - 10$ GeV bin for the north(top) and south(bottom) arm with pp data

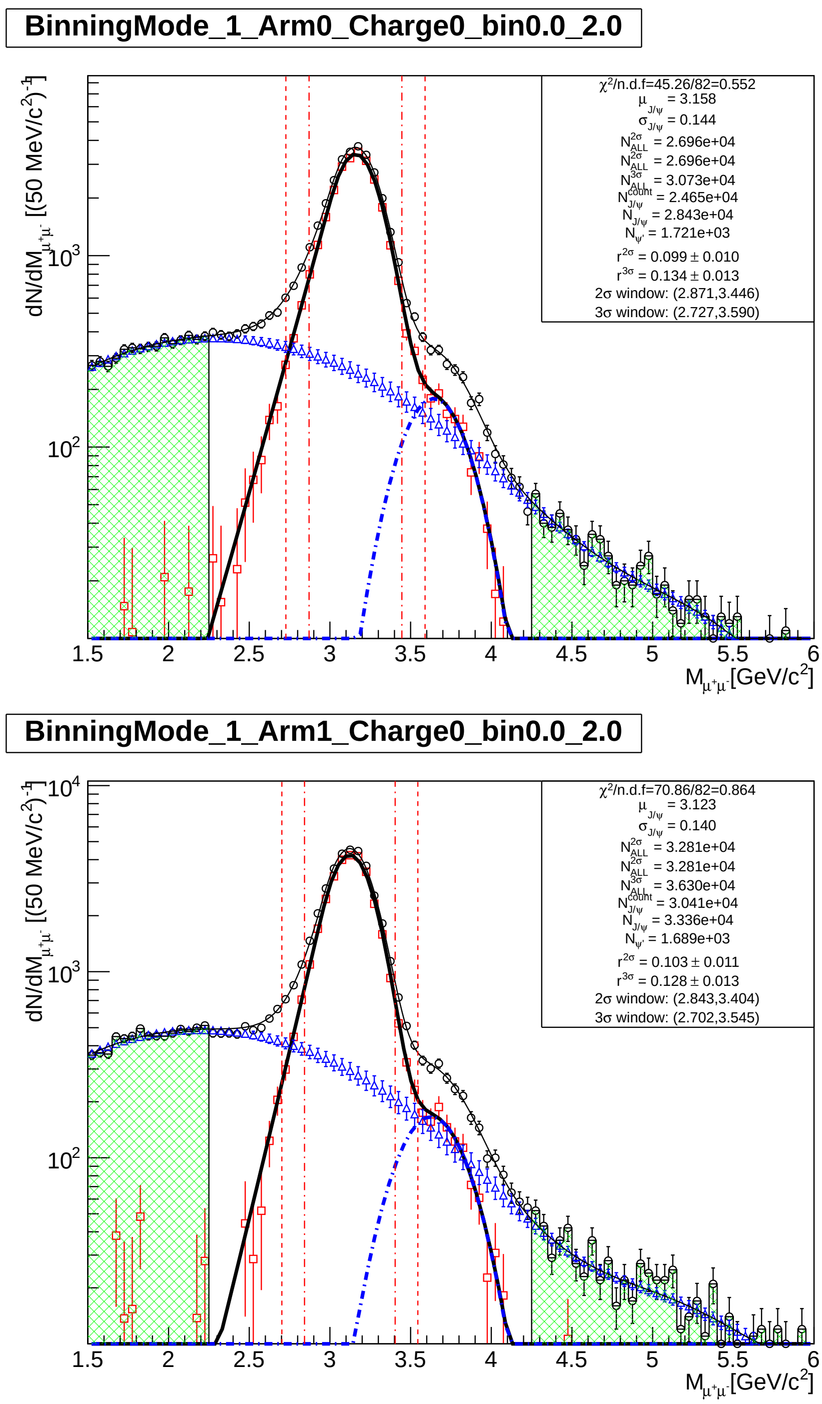

Figure 4: MuTr mass spectrum fits with GPR background estimation for $p_T = 0 - 2$ GeV bin for the north(top) and south(bottom) arm with pp data

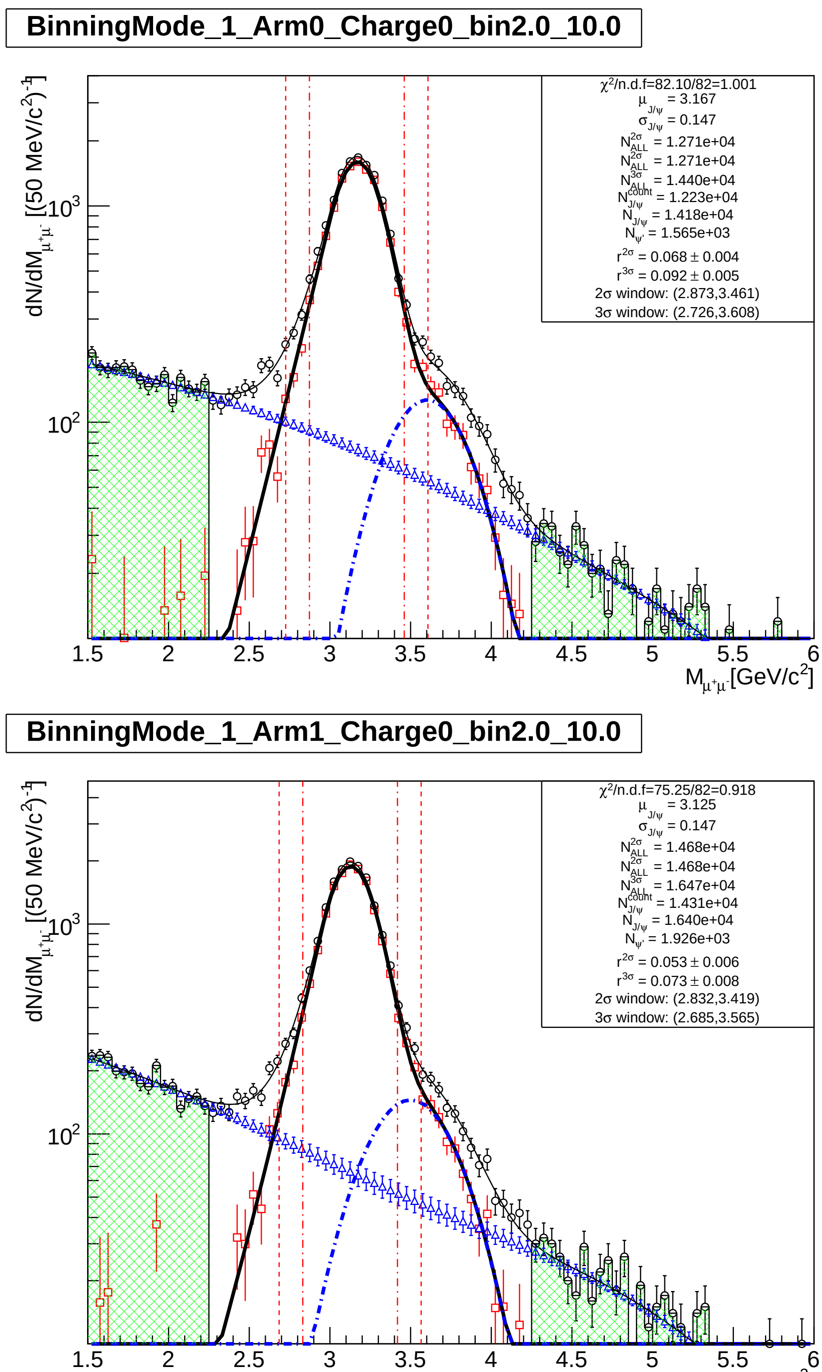

Figure 5: MuTr mass spectrum fits with GPR background estimation for $p_T = 2 - 10$ GeV bin for the north(top) and south(bottom) arm with pp data

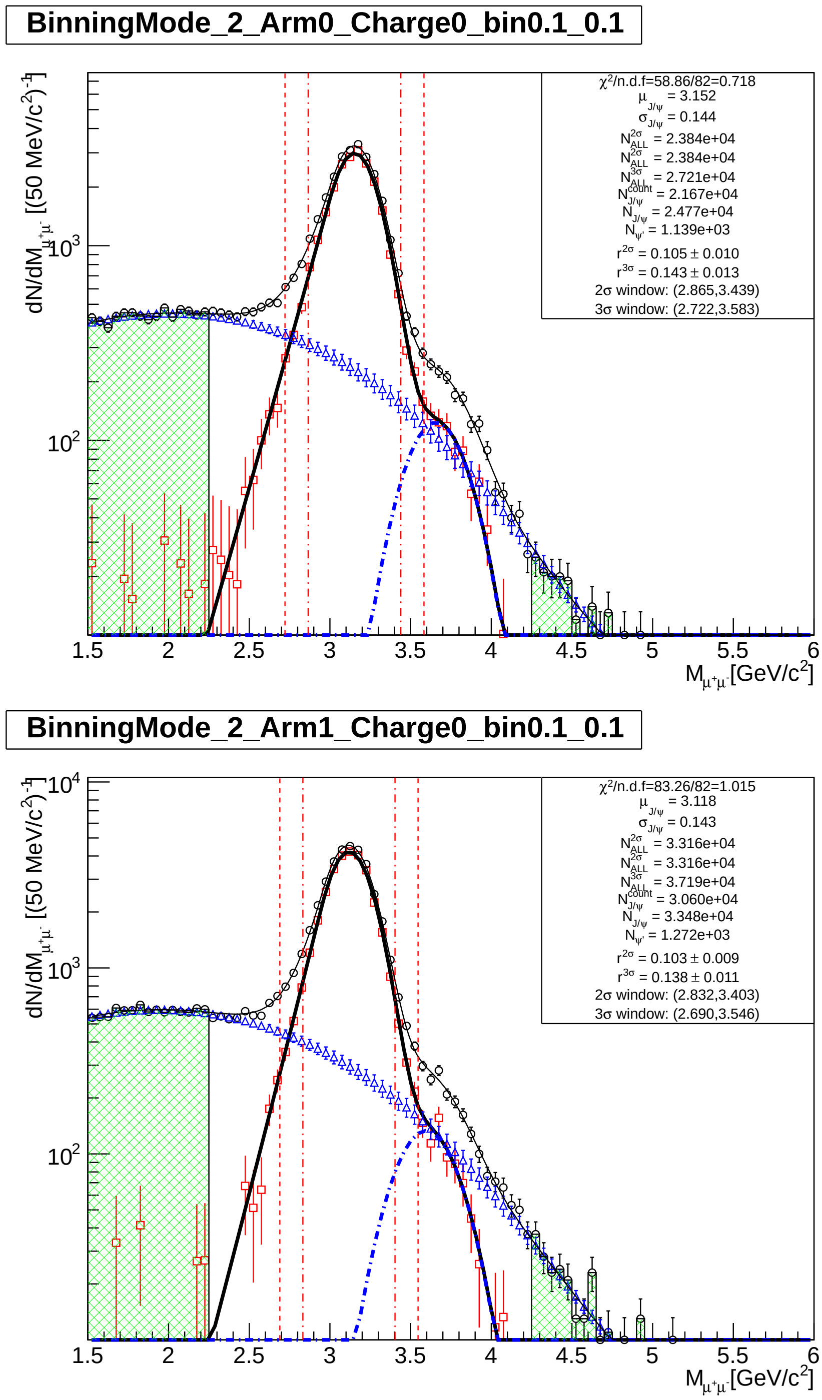

Figure 6: MuTr mass spectrum fits with GPR background estimation for $x_F = 0.05 - 0.11$ bin for the north(top) and south(bottom) arm with pp data

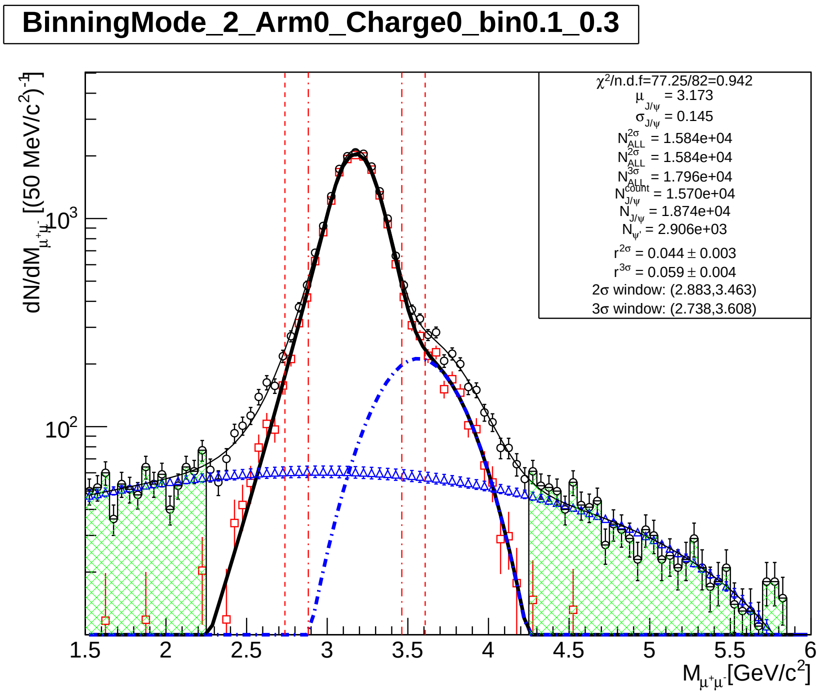

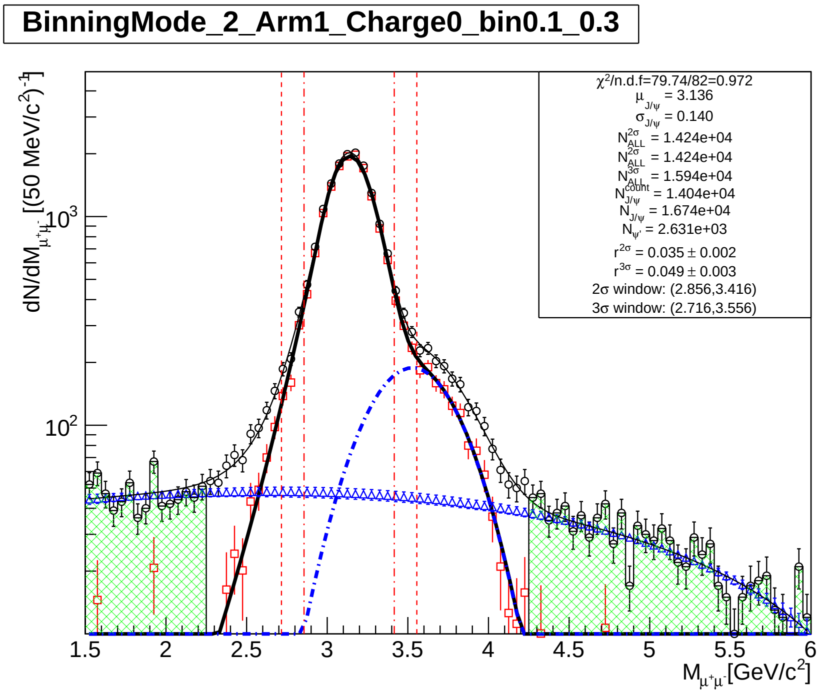

Figure 7: MuTr mass spectrum fits with GPR background estimation for $x_F = 0.11 - 0.30$ bin for the north(top) and south(bottom) arm with pp data

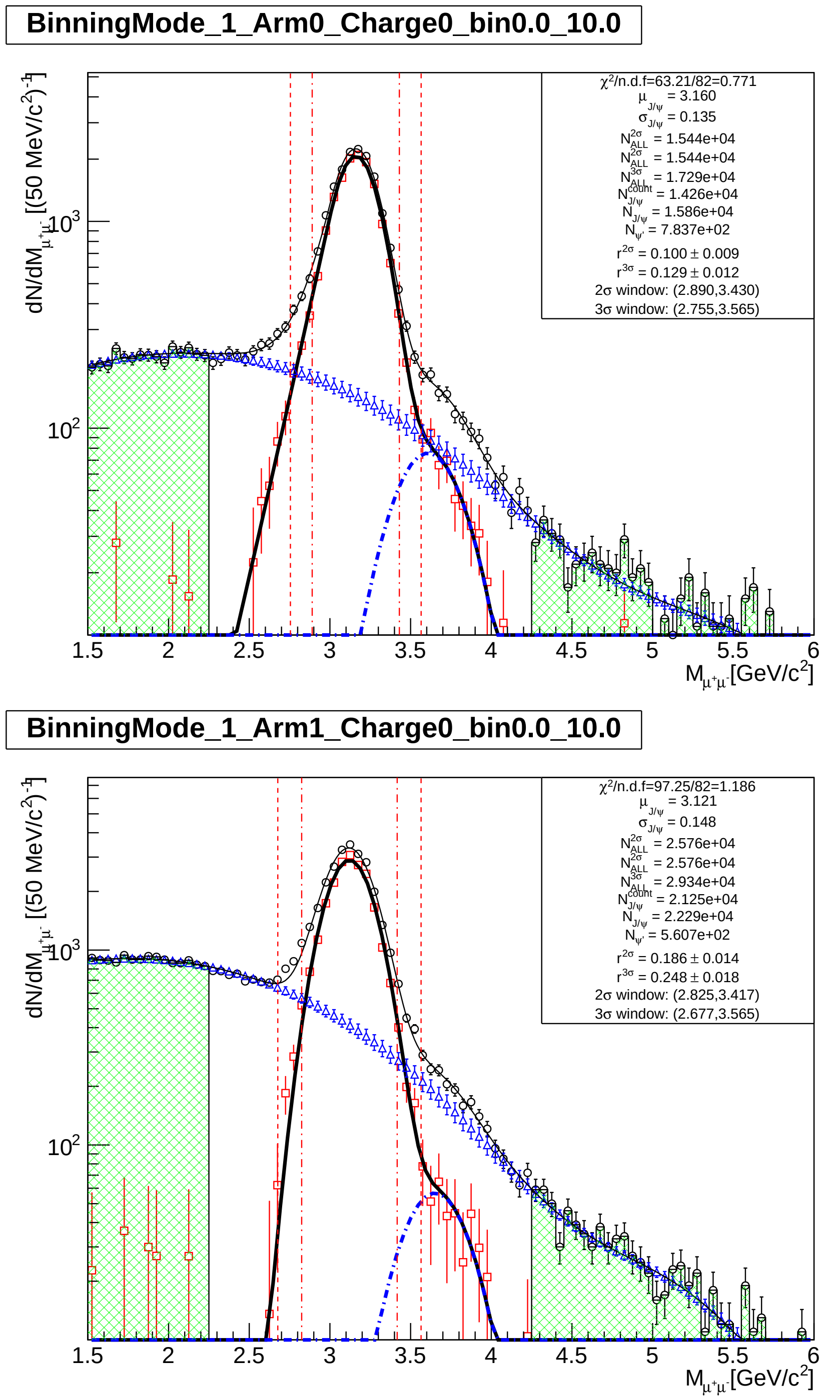

Figure 8: MuTr mass spectrum fits with GPR background estimation for $p_T = 0-10$ GeV bin for the north(top) and south(bottom) arm with pAu data

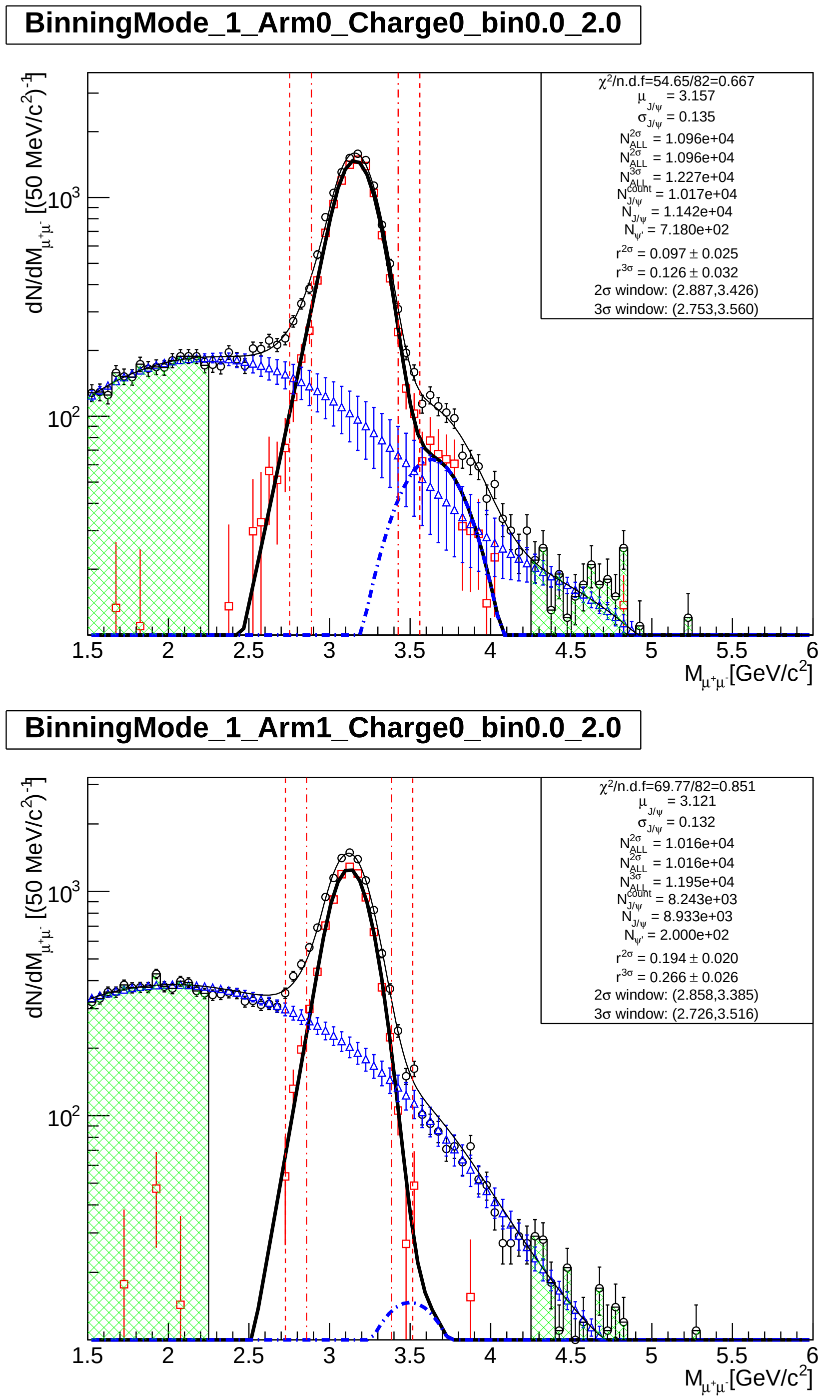

Figure 9: MuTr mass spectrum fits with GPR background estimation for $p_T = 0 - 2$ GeV bin for the north(top) and south(bottom) arm with pAu data

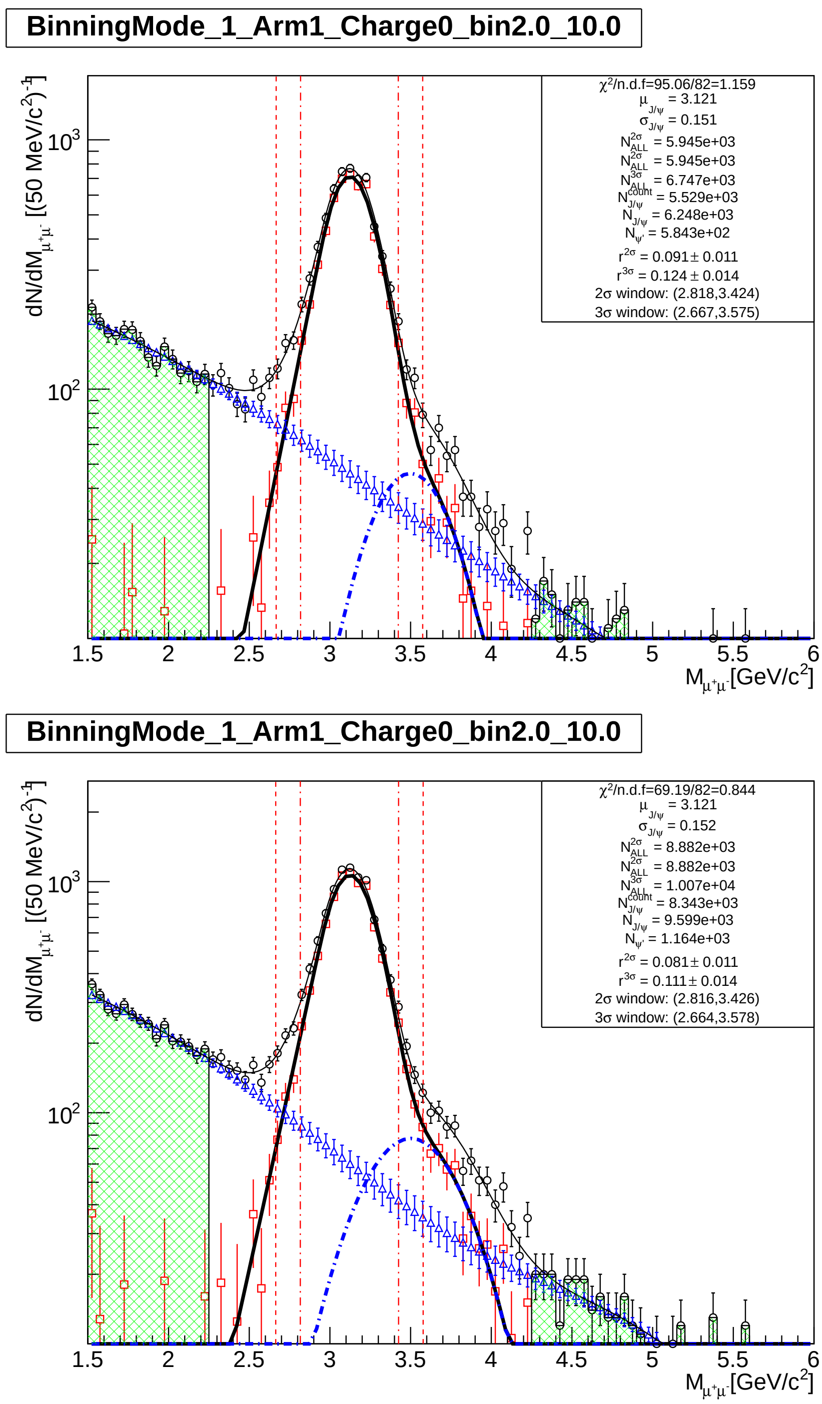

Figure 10: MuTr mass spectrum fits with GPR background estimation for $p_T = 2 - 10$ GeV bin for the north(top) and south(bottom) arm with pAu data

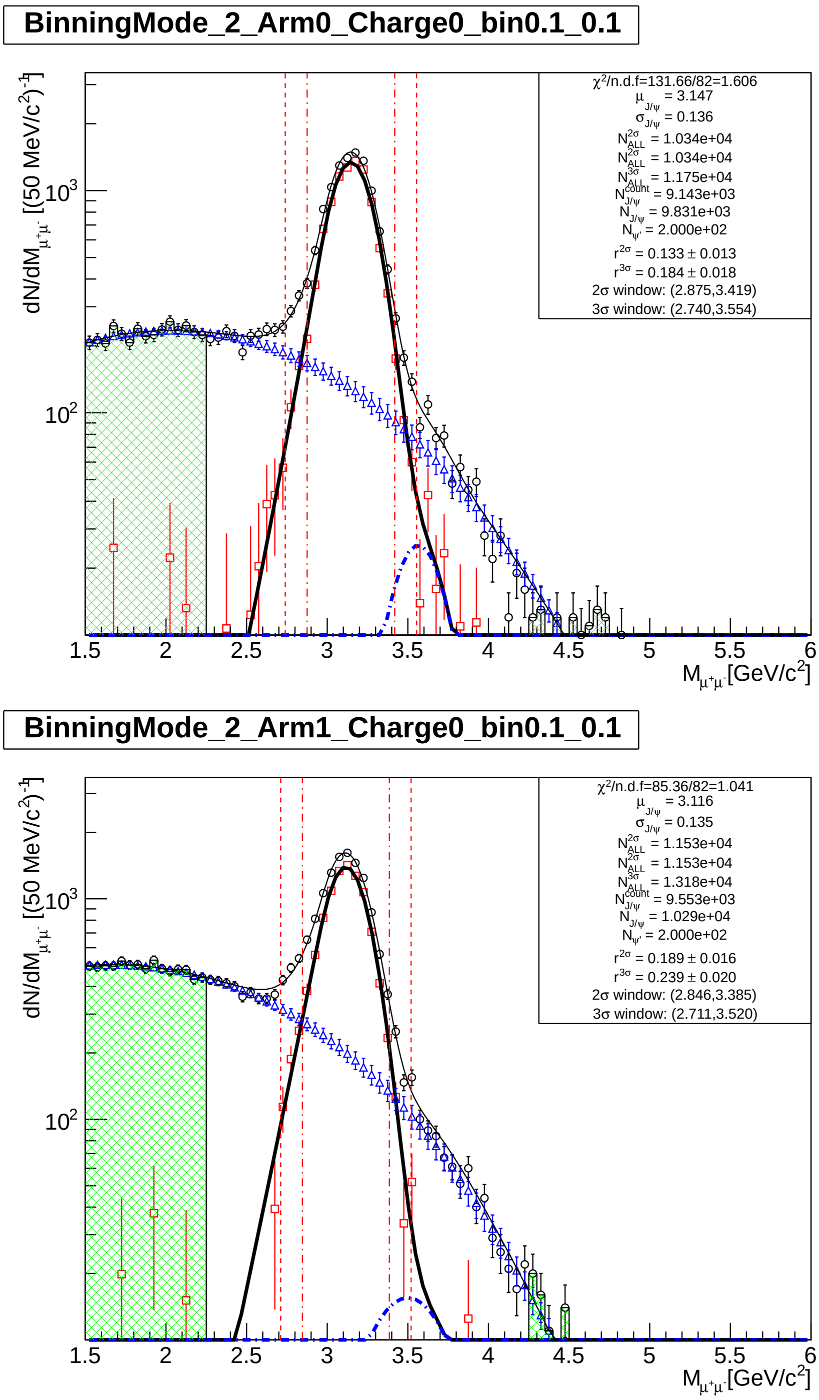

Figure 11: MuTr mass spectrum fits with GPR background estimation for $x_F = 0.05 - 0.11$ bin for the north(top) and south(bottom) arm with pAu data

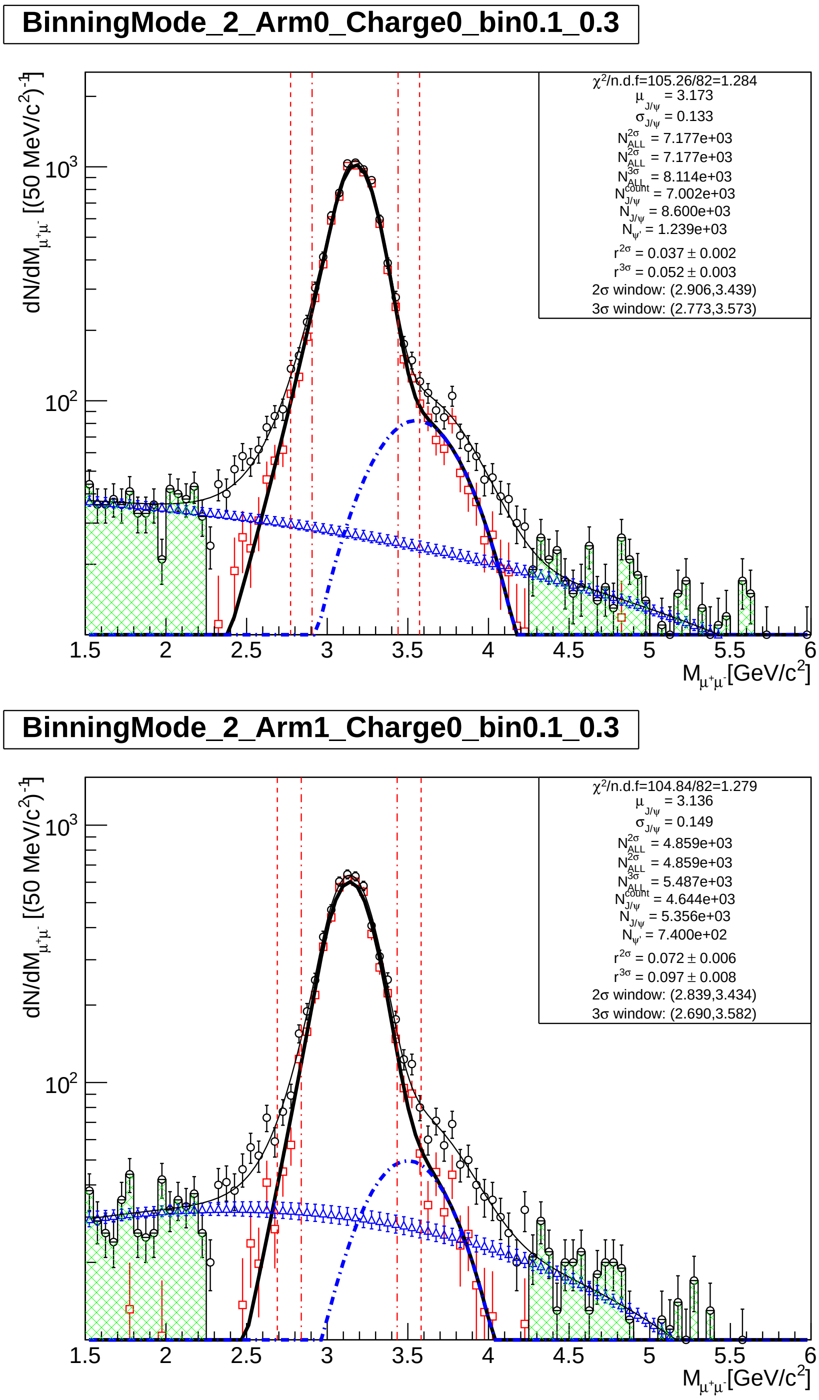

Figure 12: MuTr mass spectrum fits with GPR background estimation for $x_F = 0.11 - 0.30$ bin for the north(top) and south(bottom) arm with pAu data

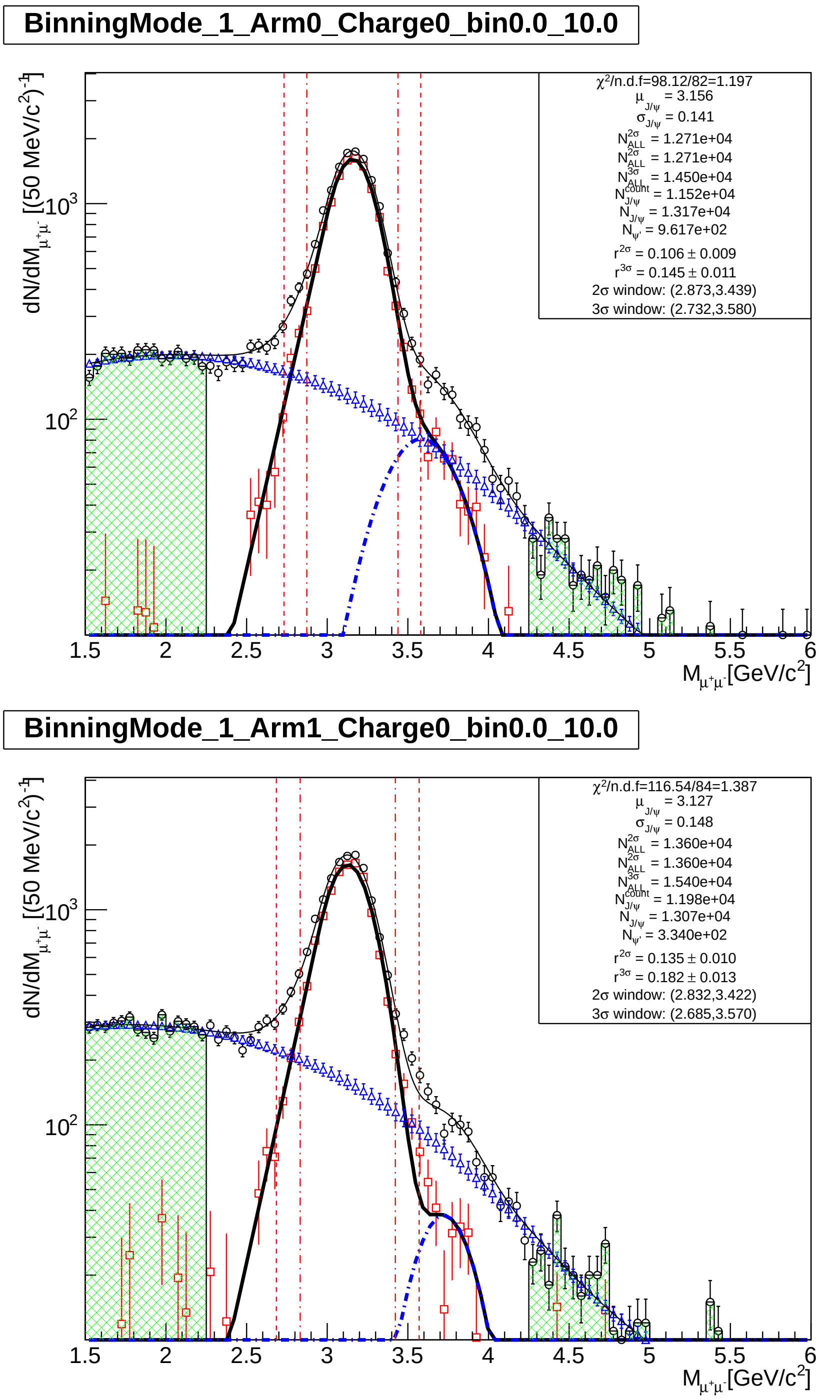

Figure 13: MuTr mass spectrum fits with GPR background estimation for $p_T = 0 - 10$ GeV bin for the north(top) and south(bottom) arm with pAl data

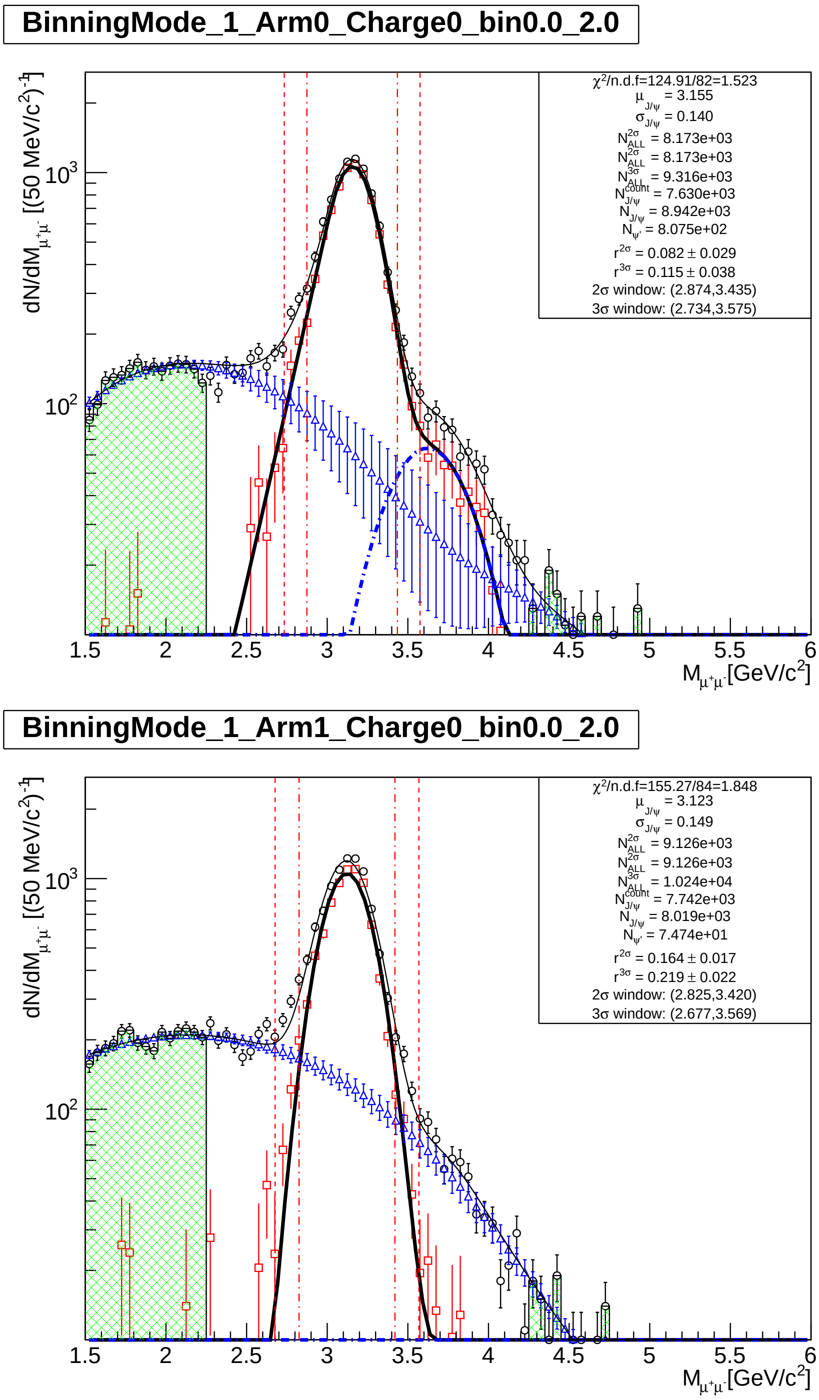

Figure 14: MuTr mass spectrum fits with GPR background estimation for $p_T = 0 - 2$ GeV bin for the north(top) and south(bottom) arm with pAl data

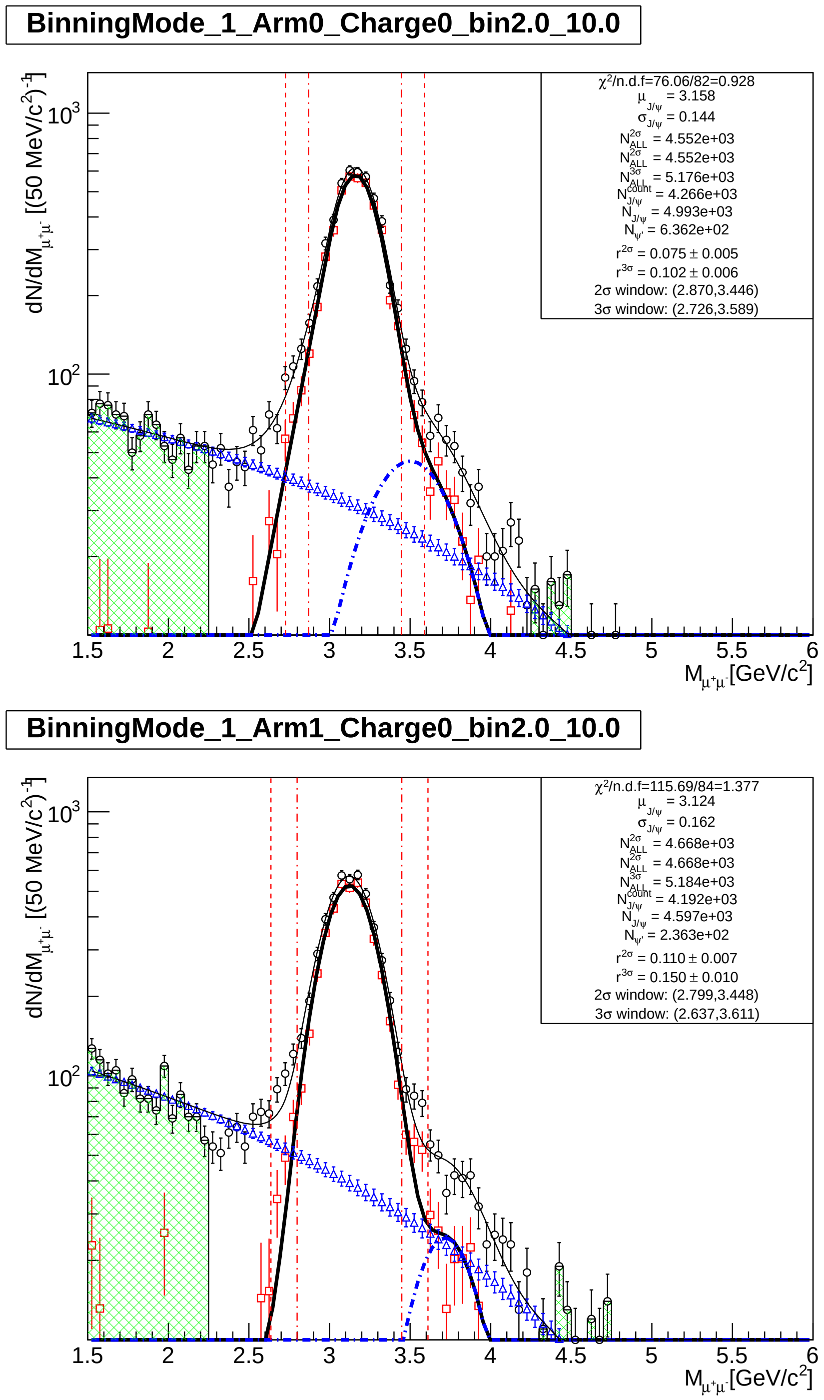

Figure 15: MuTr mass spectrum fits with GPR background estimation for $p_T = 2 - 10$ GeV bin for the north(top) and south(bottom) arm with pAl data

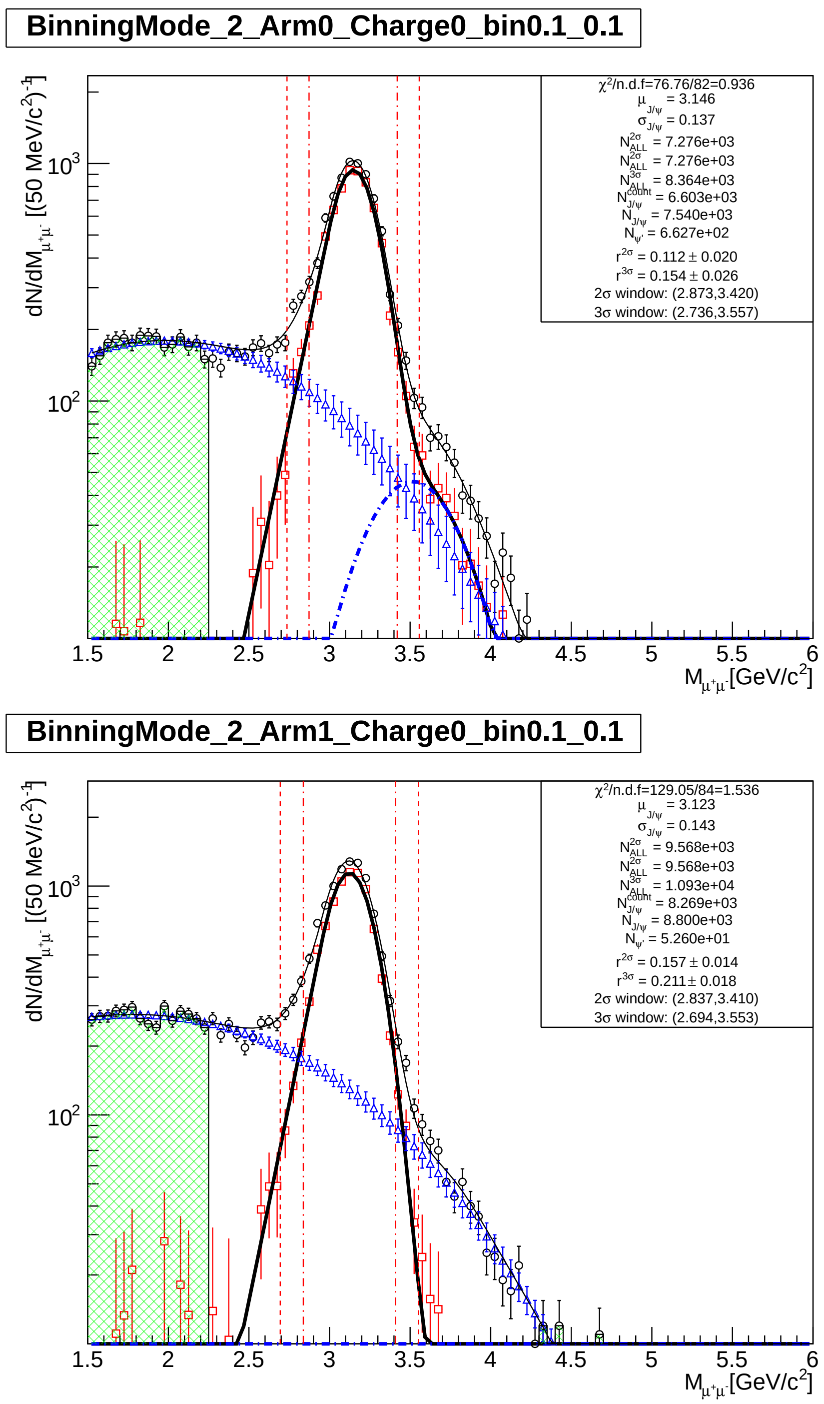

Figure 16: MuTr mass spectrum fits with GPR background estimation for $x_F = 0.05 - 0.11$ bin for the north(top) and south(bottom) arm with pAl data

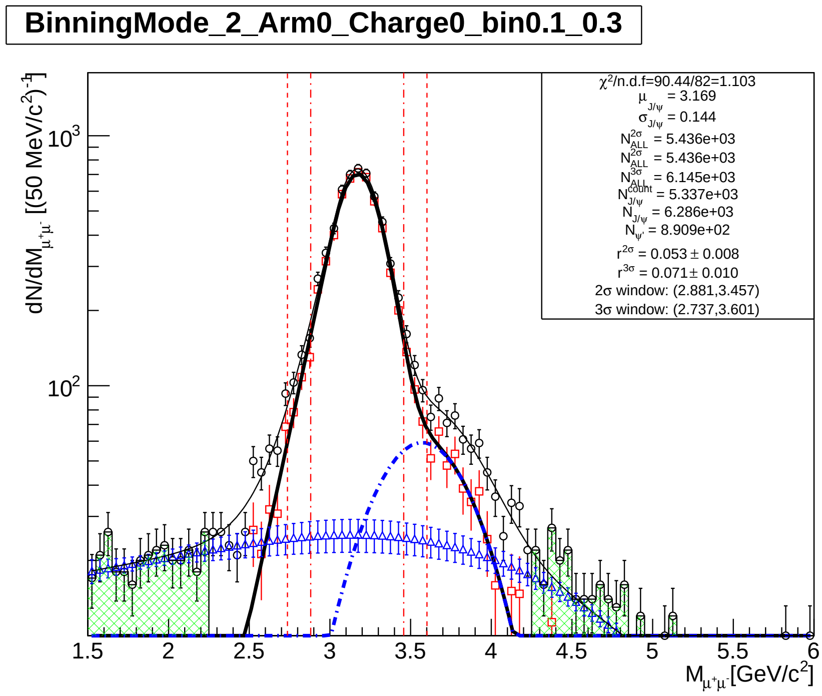

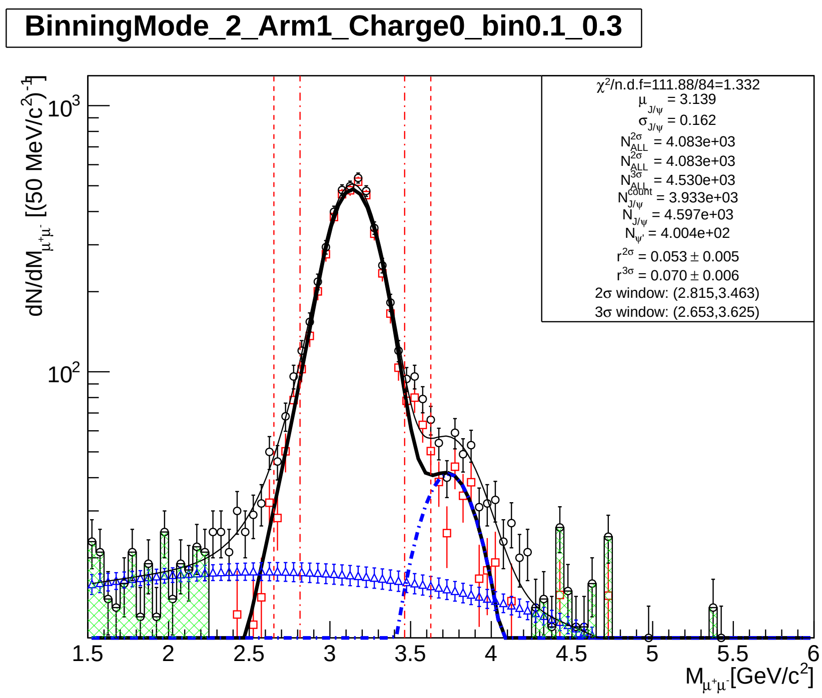

Figure 17: MuTr mass spectrum fits with GPR background estimation for $x_F = 0.11 - 0.30$ GeV bin for the north(top) and south(bottom) arm with pAl data

p_T	$f_{Bgr} \pm \delta f_{Bgr}(Stat.)(\%)$ North	$f_{Bgr} \pm \delta f_{Bgr}(Stat.)(\%)$ South
$p_T \in 0-2$	9.9 ± 1.0	10.3 ± 1.1
$p_T \in 2-10$	6.8 ± 0.7	5.3 ± 0.6

Table 1: Background Fraction in p_T bins for pp data

p_T	$f_{Bgr} \pm \delta f_{Bgr}(Stat.)(\%)$ North	$f_{Bgr} \pm \delta f_{Bgr}(Stat.)(\%)$ South
$p_T \in 0-2$	9.7 ± 1.6	19.4 ± 2.2
$p_T \in 2-10$	7.5 ± 0.5	9.1 ± 1.1

Table 2: Background Fraction in p_T bins for pAu data

p_T	$f_{Bgr} \pm \delta f_{Bgr}(Stat.)(\%)$ North	$f_{Bgr} \pm \delta f_{Bgr}(Stat.)(\%)$ South
$p_T \in 0-2$	8.2 ± 1.6	16.3 ± 1.5
$p_T \in 2-10$	7.5 ± 0.6	11.0 ± 0.7

Table 3: Background Fraction in p_T bins for pAl data

x_F	$f_{Bgr} \pm \delta f_{Bgr}(Stat.)(\%)$ North	$f_{Bgr} \pm \delta f_{Bgr}(Stat.)(\%)$ South
$x_F \in 0.05-0.11$	10.5 ± 1.0	10.3 ± 0.9
$x_F \in 0.11-0.30$	4.4 ± 0.3	3.5 ± 0.2

Table 4: Background Fraction in x_F bins for pp data

x_F	$f_{Bgr} \pm \delta f_{Bgr}(Stat.)(\%)$ North	$f_{Bgr} \pm \delta f_{Bgr}(Stat.)(\%)$ South
$x_F \in 0.05-0.11$	13.3 ± 1.6	18.9 ± 1.6
$x_F \in 0.11-0.30$	3.6 ± 0.2	7.2 ± 0.6

Table 5: Background Fraction in x_F bins for pAu data

x_F	$f_{Bgr} \pm \delta f_{Bgr}(Stat.)(\%)$ North	$f_{Bgr} \pm \delta f_{Bgr}(Stat.)(\%)$ South
$x_F \in 0.05-0.11$	11.2 ± 2.5	15.7 ± 1.6
$x_F \in 0.11-0.30$	5.3 ± 0.6	5.3 ± 0.5

Table 6: Background Fraction in x_F bins for pAl data

4 J/ψ Transverse Single Spin Asymmetry

Equation 1, 2 shows how we extract the physics J/ψ double spin Asymmetry

$$A_N^{J/\psi} = \frac{A_N^{incl} - f \cdot A_N^{bgr.}}{1-f} \quad (1)$$

$$\delta A_N^{J/\psi} = \frac{\sqrt{(\delta A_N^{incl})^2 + f^2 \cdot (\delta A_N^{bgr})^2}}{1-f} \quad (2)$$

where f = N^{BG}/N^{incl} is the background fraction which comes from section 3. A_N^{inc} is the inclusive dimuon asymmetry within 2 σ mass window cut. $A_N^{bgr.}$ is the background asymmetry which we estimate from the low side band dimuon and the mass range of which is from 1.5GeV to 2.4GeV.

5 Maximum Likelihood method

Maximum likelihood method has been used in the previous J/ψ A_N analysis and it has the advantage of dealing with low statistic situation. A detailed description of this method can be found in K. Oleg Eyser's analysis note 1018. Here exactly the same likelihood function is used here and shown in equation 11 and 12. As we have described in section 6.1, when dealing with yellow bin, $\pi - \phi$ is put into the equations below instead of ϕ.

For spin up:

$$-logL(\phi) = -\sum log(1 + \epsilon * cos(\phi_i)) \quad (3)$$

For spin down:

$$-logL(\phi) = -\sum log(1 - \epsilon * cos(\phi_i)) \quad (4)$$

A scanning of ϵ from -0.6 to 0.6 with 1200 steps has been proceeded for finding the best estimator (ϵ_{best}). Having got the best estimator, the asymmetry can be calculated by $A_N = \epsilon_{best}$/Polarization, where Polarization is the average polarization of each run weighted by run luminosity.

One more thing needed to be mentioned here is the spin value read from Spin Data Base. The values in the spin DB are taken from CDEV packets, which is provided by CAD. CDEV data has spin information at 12'o clock, where the RHIC polarimeters are located. Therefore, +1(-1) in the spin DB means spin-down (spin-up) at 12 o'clock.

The spin direction is reversed at PHENIX after the proton beam passed the Siberian snakes(helical magnets) between 12'o clock and PHENIX (there are two places where the Siberian snakes are in the RHIC, so the spin direction is back to original after each rotation). Therefore, +1(-1) in the spin DB means spin-down(spin-up) at PHENIX.

5.1 Maximum Likelihood method with pp data

In pp collision, both blue beam and yellow beam are polarized. In Run15, the transverse polarization direction is along Y-axis. So when $A_N(\phi)$ is calculated w.r.t blue beam, the azimuthal angle is already under PHENIX coordinate system. However, this is not the case for yellow beam since yellow beam is traveling towards South Arm which is along the negative Z direction in PHENIX coordinate system. The azimuthal angle under PHENIX coordinate system is $\pi - \phi$ w.r.t yellow beam. Therefore, instead of fitting with $\cos(\phi)$ we fit $A_N(\phi)$ with $\cos(\pi - \phi)$ when dealing with yellow beam related A_N.

Table 7 and 8 list the inclusive(background) A_N with all the bins for Blue and Yellow beam. The difference of $A_N^{Incl.(bgr)}$ between Spin Analyzer and Maximum Likelihood method for each bin is around 0.1 sigma which is in a reasonable range.

Arm (Blue Beam)	A_N^{incl}	A_N^{bgr}
North($0 < p_T < 2GeV$)	0.007 ± 0.015	0.032 ± 0.035
North($2 < p_T < 10GeV$)	0.016 ± 0.021	0.111 ± 0.058
North($0.05 < x_F < 0.11GeV$)	0.005±0.015	0.035±0.032
North($0.11 < x_F < 0.30GeV$)	0.016±0.019	0.178±0.087
South($0 < p_T < 2Gev$)	0.004 ± 0.013	0.023 ± 0.028
South($2 < p_T < 10Gev$)	0.011 ± 0.020	0.005 ± 0.056
South($0.05 < x_F < 0.11GeV$)	0.004±0.013	0.025±0.026
South($0.11 < x_F < 0.30GeV$)	0.015±0.020	-0.023±0.096

Table 7: List of Inclusive and background A_N from Maximum Likelihood for Blue beam with pp data

Arm(Yellow Beam)	A_N^{incl}	A_N^{bgr}
North($0 < p_T < 2GeV$)	0.021 ± 0.015	0.018 ± 0.035
North($2 < p_T < 10GeV$)	0.053 ± 0.021	0.072 ± 0.058
North($0.05 < x_F < 0.11GeV$)	0.026±0.015	0.021±0.032
North($0.11 < x_F < 0.30GeV$)	0.040±0.019	0.117±0.087
South($0 < p_T < 2Gev$)	0.005 ± 0.013	0.032 ± 0.030
South($2 < p_T < 10Gev$)	0.004 ± 0.020	0.060 ± 0.056
South($0.05 < x_F < 0.11GeV$)	0.009±0.013	0.029±0.028
South($0.11 < x_F < 0.30GeV$)	-0.005±0.020	0.137±0.096

Table 8: List of Inclusive and background A_N from Maximum Likelihood for Yellow beam with pp data

5.2 Maximum Likelihood method with pAu data

In pAu, only proton is polarized and traveling towards positive Z direction so the azimuthal angle is already under PHENIX coordinate system.

5.2.1 Tilt angle correction

Figure 18 Shows the $FVTX_X vs. FVTX_Z$ distribution in pp collision where two proton are moving along z-axis and no tilt angle exist there. In that case, the highlight band is perpendicular to x-axis. In pAu collision, it is still head-down collision. But we observed a tilt angle in X-Z plane which can be seen from figure 19. And the tilt angle is 3.6 mrad which is given by CAD published paper.

This tilt angle makes the CM frame of collision no longer in PHENIX coordinate system. Since every quantity is recorded under PHENIX coordinate system, we need to transform 3-D vector, momentum in this case, into CM frame. Since it is still head-down collision, only rotation transformation is needed for this purpose. The transformation is shown as following:

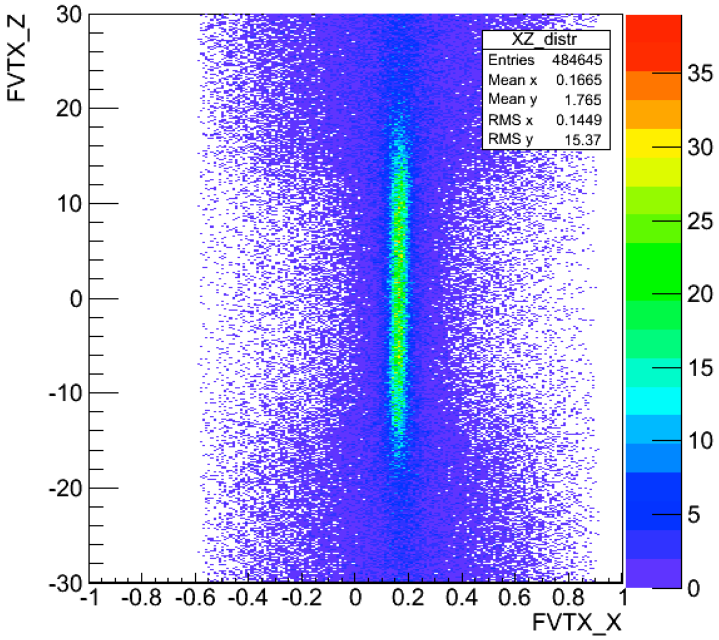

Figure 18: This plot shows FVTX_X vs. FVTX_Z distribution in pp collision. The tilt highlight band is perpendicular to x-axis which indicates that pp collision in Run15 is along Z-axis.

$$p'_y = p_y \tag{5}$$

$$p'_x = \cos(\alpha) * p_x - \sin(\alpha) * p_z \tag{6}$$

$$p'_z = \sin(\alpha) * p_x + \cos(\alpha) * p_z \tag{7}$$

where $p_{x,y,z}$ is the momentum recorded in pDST and $p'_{x,y,z}$ is the momentum in CM frame and α is 3.6 mrad as mentioned above.

This tilt angle will not affect the result in the leading order. A comparison has been made between inclusive and background A_N before and after tilt angle

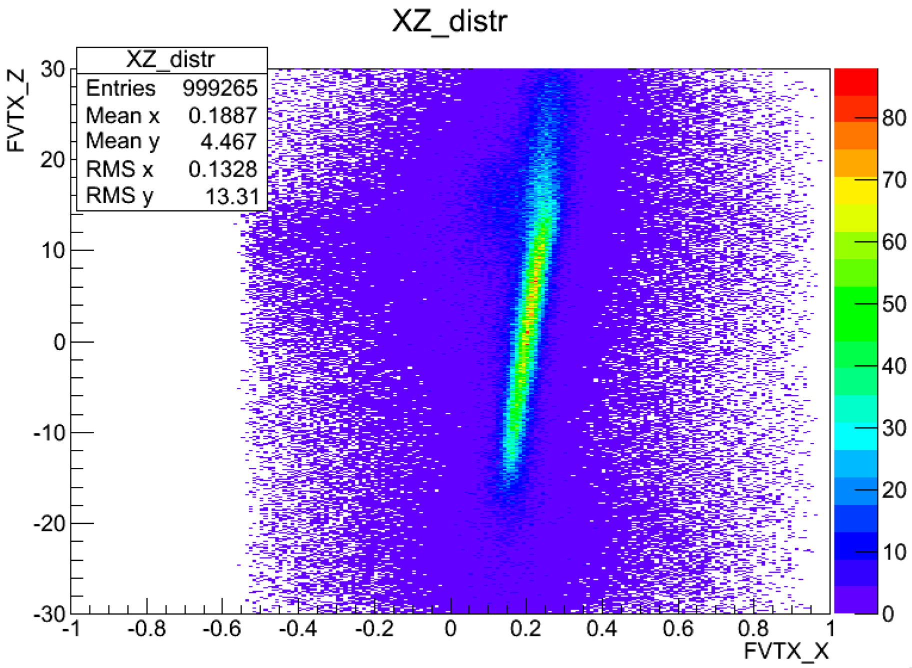

Figure 19: This plot shows FVTX_X vs. FVTX_Z distribution in pAu collision. The tilt highlight band indicates that pAu collision is not exactly along Z-axis.

correction. Figure 20 shows the inclusive and background A_N in x_F bin before tilt angle correction. The fluctuation due to the tilt angle correction is about 0.1 sigma.

5.2.2 Inclusive and background A_N with pAu data after tilt angle correction

Figure 21 shows inclusive and background asymmetry scanning with Maximum Likelihood method for $p+\mathrm{Au}$ data. Table 9 and 10 list the inclusive and background A_N that we found from the scanning.

p_T	$A_N^{Inc.} \pm \delta A_N^{Inc.}(Stat.)$ North	$A_N^{Inc.} \pm \delta A_N^{Inc.}(Stat.)$ South
$p_T \in 0-2$	-0.061 ± 0.022	-0.056 ± 0.023
$p_T \in 2-10$	0.010 ± 0.028	0.010 ± 0.028
$x_F \in 0.05-0.11$	-0.025±0.023	-0.045±0.021
$x_F \in 0.11-0.30$	-0.045±0.027	-0.021±0.033

Table 9: $A_N^{Inc.}$ in different p_T and x_F bins with pAu data

5.3 Maximum Likelihood method with pAl data

Similar with what has been saw in pAu data, there is also a tilt angle in pAl collision and the tilt angle in pAl case is 2.5mrad. The result shown in this

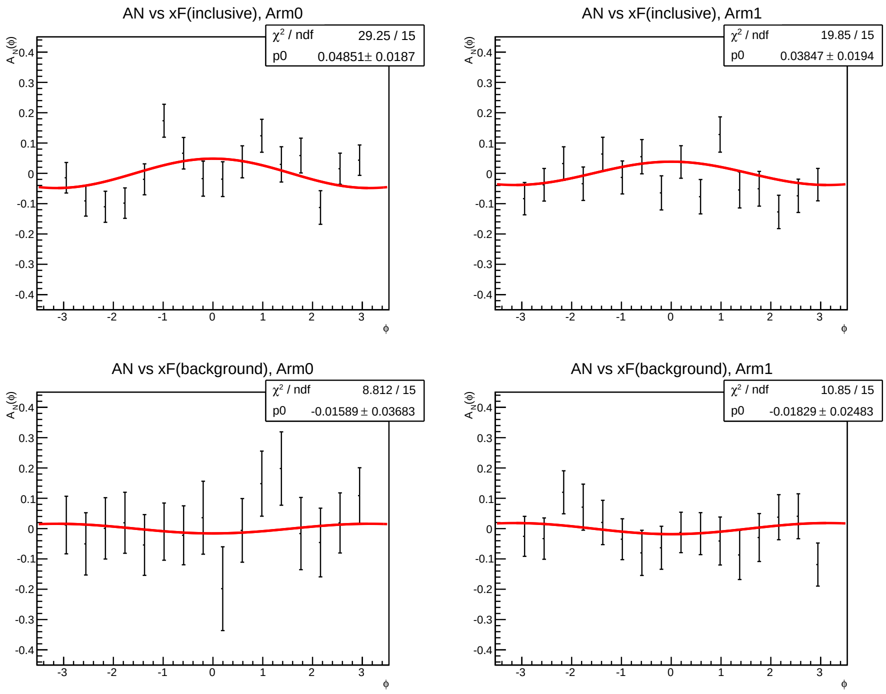

Figure 20: A_N for all x_F before tilt angle correction.

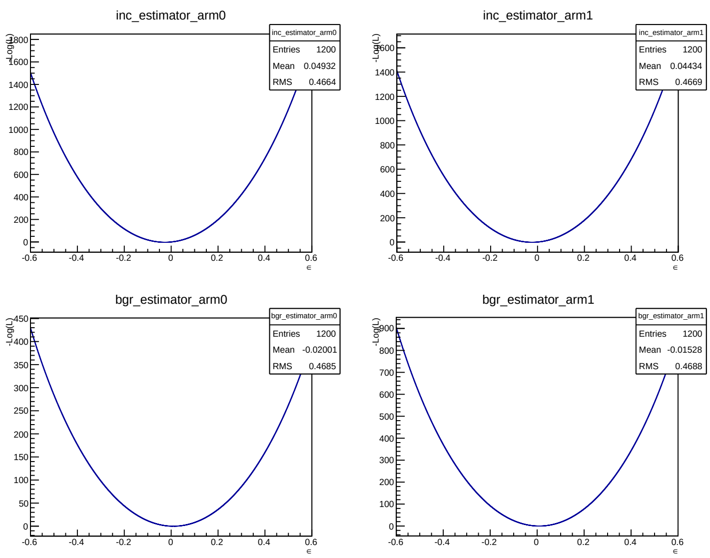

Figure 21: Epsilon scanning with pAu dataset. Top(bottom) left: epsilon scanning for inclusive(background) A_N in North arm with $0.05 < x_F < 0.11$. Top(bottom) right: epsilon scanning for inclusive(background) A_N in South arm with $0.05 < x_F < 0.11$.

p_T	$A_N^{Bgr.} \pm \delta A_N^{Bgr.} (Stat.)$ North	$A_N^{Bgr.} \pm \delta A_N^{Bgr.} (Stat.)$ South
$p_T \in 0 - 2$	-0.005 ± 0.043	0.020 ± 0.028
$p_T \in 2 - 10$	-0.026 ± 0.055	-0.017 ± 0.046
$x_F \in 0.05 - 0.11$	-0.010 ± 0.036	0.015 ± 0.025
$x_F \in 0.11 - 0.30$	-0.036 ± 0.093	-0.051 ± 0.097

Table 10: $A_N^{Bgr.}$ in different p_T and x_F bins with pAu data

section is the inclusive and background A_N after the tilt angle correction.

Figure 21 and 22 show inclusive and background asymmetry scanning with Maximum Likelihood method for $p +$ Al data. Table 11 and 12 lists the inclusive and background A_N that we found from the scanning.

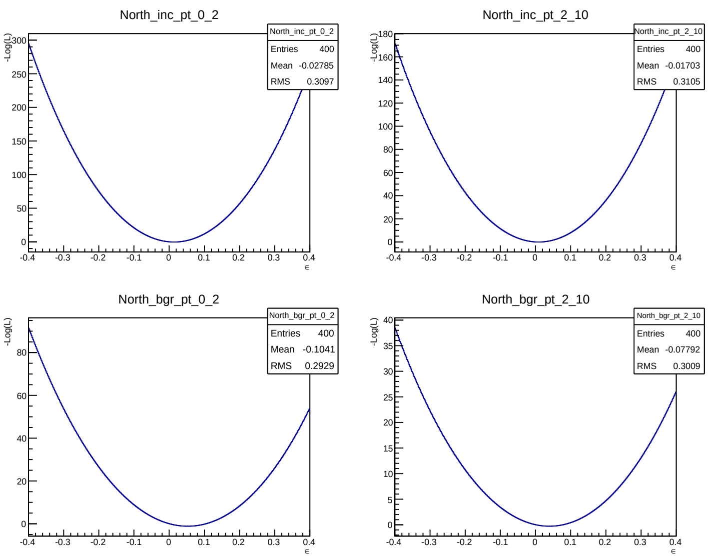

Figure 22: Epsilon scanning with pAl dataset. Top(bottom) left: epsilon scanning for inclusive A_N in North arm with $0 < p_T < 2GeV$. Top(bottom) right: epsilon scanning for background A_N in North arm with $2 < p_T < 10GeV$.

p_T	$A_N^{Inc.} \pm \delta A_N^{Inc.} (Stat.)$ North	$A_N^{Inc.} \pm \delta A_N^{Inc.} (Stat.)$ South
$p_T \in 0 - 2$	0.031 ± 0.027	-0.018 ± 0.026
$p_T \in 2 - 10$	0.002 ± 0.037	0.051 ± 0.036
$x_F \in 0.05 - 0.11$	0.023 ± 0.029	-0.009±0.025
$x_F \in 0.11 - 0.30$	0.025 ± 0.037	0.042± 0.038

Table 11: $A_N^{Inc.}$ in different p_T and x_F bins with pAl data

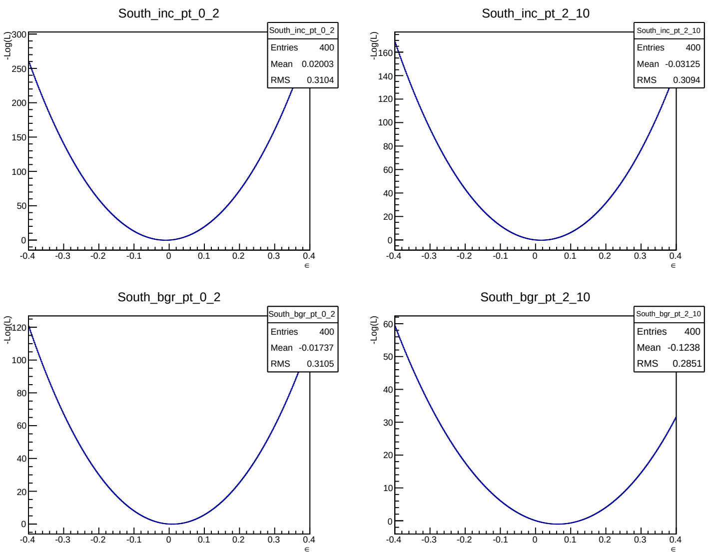

Figure 23: Epsilon scanning with pAl dataset. Top(bottom) left: epsilon scanning for inclusive A_N in South arm with $0 < p_T < 2GeV$. Top(bottom) right: epsilon scanning for background A_N in South arm with $2 < p_T < 10GeV$.

p_T	$A_N^{Bgr.} \pm \delta A_N^{Bgr.}(Stat.)$ North	$A_N^{Bgr.} \pm \delta A_N^{Bgr.}(Stat.)$ South
$p_T \in 0-2$	0.090 ± 0.050	-0.029 ± 0.048
$p_T \in 2-10$	0.113 ± 0.077	0.009 ± 0.084
$x_F \in 0.05-0.11$	0.091 ± 0.044	-0.040± 0.043
$x_F \in 0.11-0.30$	0.093± 0.129	0.234±0.152

Table 12: $A_N^{Bgr.}$ in different p_T and x_F bins with pAl data

5.4 $J/\psi A_N$

Having obtained the inclusive and background asymmetries the signal asymmetry can be calculated from Equation 1 and Equation 2. Figure 24 to 25 show $J/\psi A_N$ in different p_T and x_F bins with pp data. Figure 30 and 31 show $J/\psi A_N$ in different p_T and x_F bins with pAl data and figure 27 and 28 show $J/\psi A_N$ in different p_T and x_F bins with pAu data. And table 13, 14, 15 and 16 list the $J/\psi A_N$ in each arm for each p_T and x_F bin with pp, pAl and pAu data.

p_T	$A_N^{J/\psi} \pm \delta A_N^{J/\psi}(Stat.)$ North	$A_N^{J/\psi} \pm \delta A_N^{J/\psi}(Stat.)$ South
$p_T \in 0-2$	0.004 ± 0.017	0.013 ± 0.011
$p_T \in 2-10$	0.009 ± 0.023	0.011 ± 0.021
$x_F \in 0.05-0.11$	0.002 ± 0.027	0.001 ± 0.015
$x_F \in 0.11-0.30$	0.008 ± 0.021	0.017 ± 0.021

Table 13: $A_N^{J/\psi}$ in different p_T and x_F bins for Blue beam with pp data

p_T	$A_N^{J/\psi} \pm \delta A_N^{J/\psi}(Stat.)$ North	$A_N^{J/\psi} \pm \delta A_N^{J/\psi}(Stat.)$ South
$p_T \in 0-2$	0.021 ± 0.017	0.002 ± 0.015
$p_T \in 2-10$	0.051 ± 0.023	0.000 ± 0.021
$x_F \in 0.05-0.11$	0.027 ± 0.018	0.006 ± 0.015
$x_F \in 0.11-0.30$	0.037 ± 0.021	-0.010 ± 0.021

Table 14: $A_N^{J/\psi}$ in different p_T and x_F bins for Yellow beam with pp data

p_T	$A_N^{J/\psi} \pm \delta A_N^{J/\psi}(Stat.)$ North	$A_N^{J/\psi} \pm \delta A_N^{J/\psi}(Stat.)$ South
$p_T \in 0-2$	0.018 ± 0.037	-0.013 ± 0.037
$p_T \in 2-10$	-0.008 ± 0.045	0.031 ± 0.046
$x_F \in 0.05-0.11$	0.018 ± 0.039	0.062 ± 0.037
$x_F \in 0.11-0.30$	0.022 ± 0.039	-0.076 ± 0.042

Table 15: $A_N^{J/\psi}$ in different p_T and x_F bins for Blue beam with pAl data

p_T	$A_N^{J/\psi} \pm \delta A_N^{J/\psi}(Stat.)$ North	$A_N^{J/\psi} \pm \delta A_N^{J/\psi}(Stat.)$ South
$p_T \in 0-2$	-0.067 ± 0.025	-0.074 ± 0.029
$p_T \in 2-10$	0.013 ± 0.031	0.012 ± 0.033
$x_F \in 0.05-0.11$	-0.027 ± 0.027	-0.058 ± 0.027
$x_F \in 0.11-0.30$	-0.045 ± 0.029	-0.019 ± 0.037

Table 16: $A_N^{J/\psi}$ in different p_T and x_F bins for Blue beam with pAu data

6 Cross Check

First of all, it is necessary to cross check the BBC counts and dimuon yield (figure 32 to 35) for each bunch in each run. Make sure that we deal with the

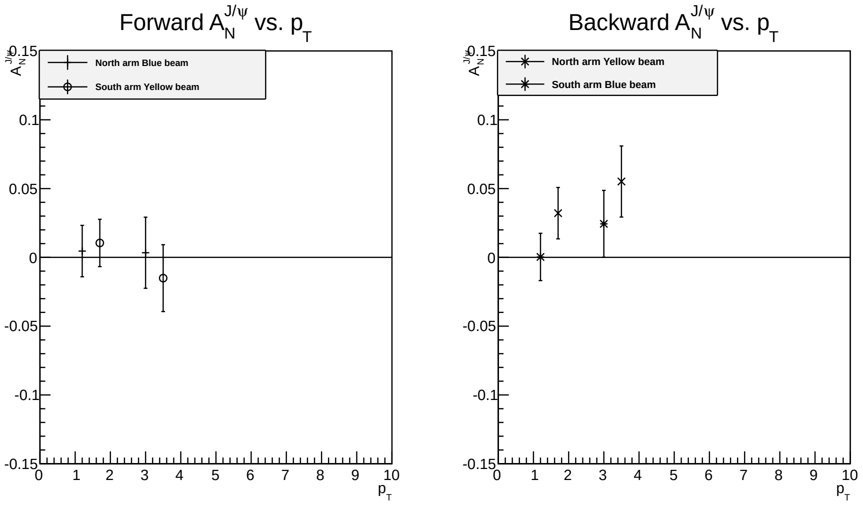

Figure 24: pp $A_N^{J/\psi}$ vs. p_T bins

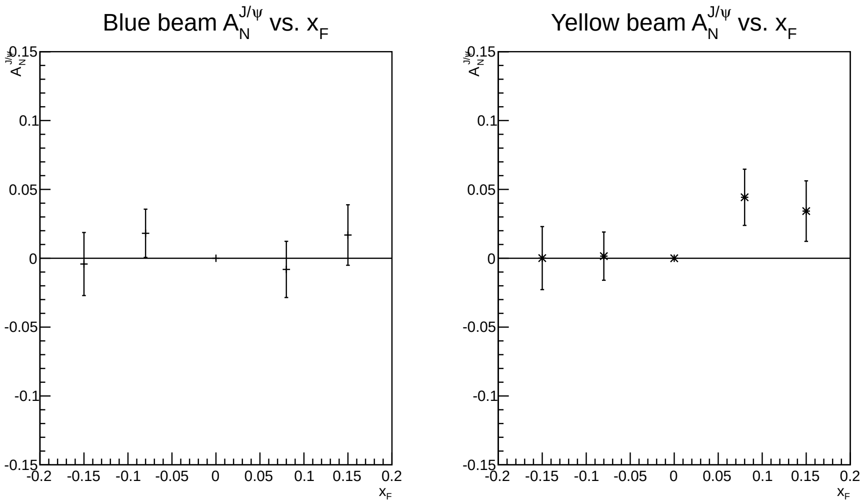

Figure 25: pp $A_N^{J/\psi}$ vs. x_F

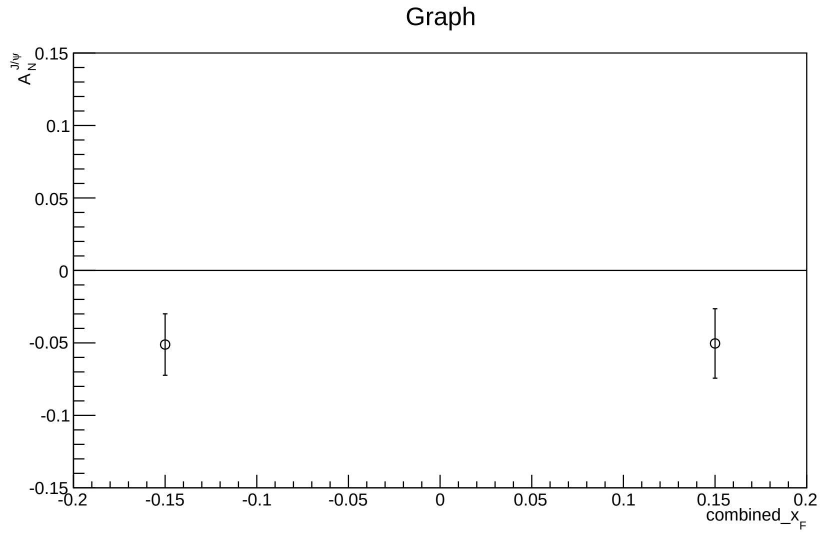

Figure 26: pAu $A_N^{J/\psi}$ in combined p_T bin

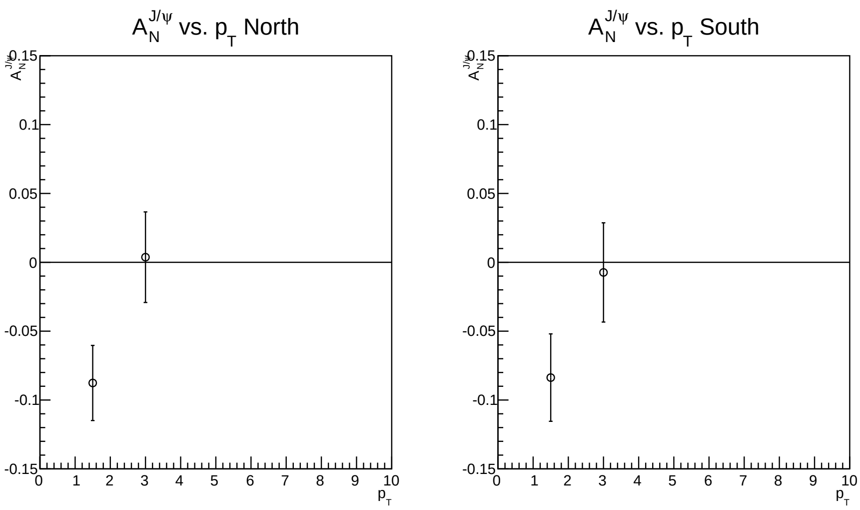

Figure 27: pAu $A_N^{J/\psi}$ vs. p_T

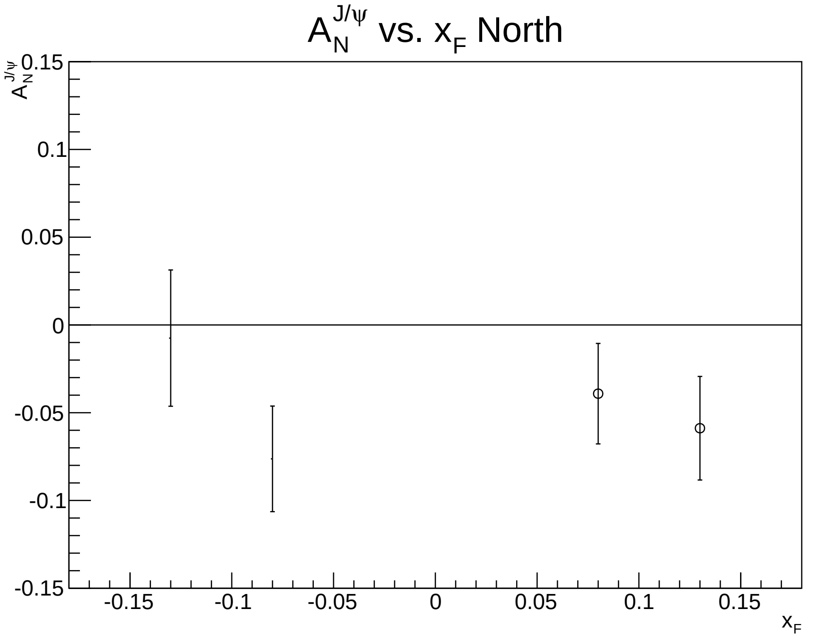

Figure 28: pAu $A_N^{J/\psi}$ vs. x_F

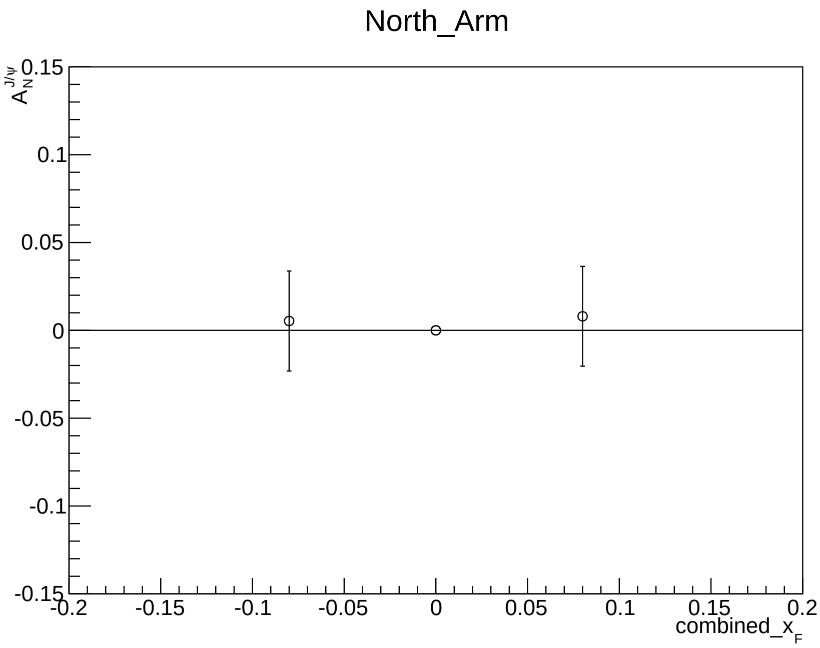

Figure 29: pAl $A_N^{J/\psi}$ in combined p_T bin

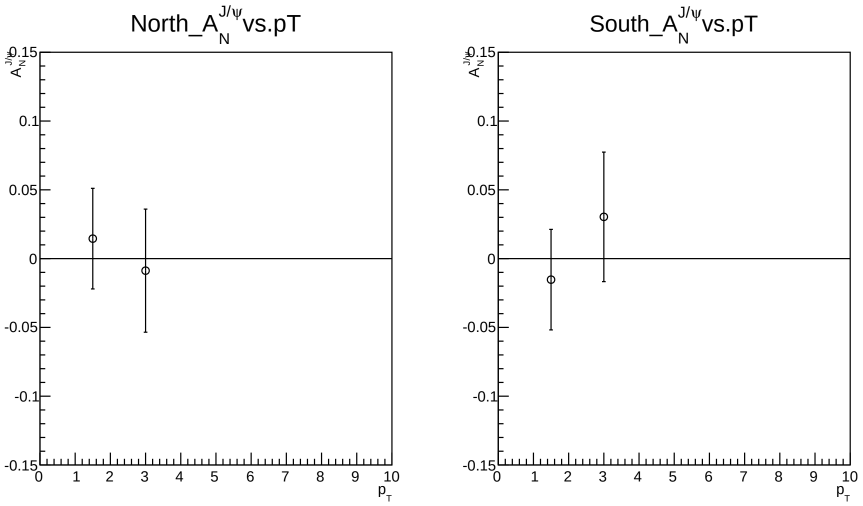

Figure 30: pAl $A_N^{J/\psi}$ vs. p_T

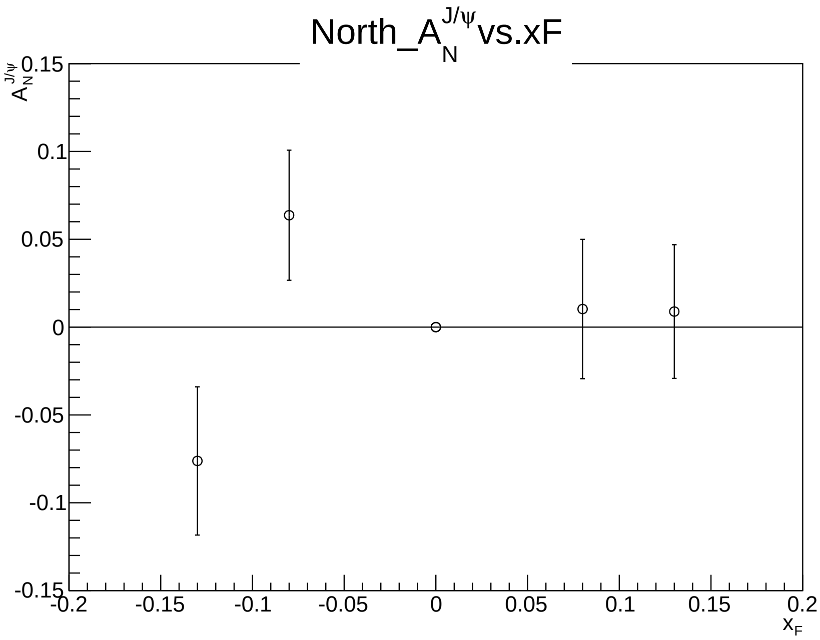

Figure 31: pAl $A_N^{J/\psi}$ vs. x_F

bunch crossing number correctly and the BBC counts read from Spin Database is reasonable.

From those plots, the abort gap can be clearly seen there and it is placed in the right crossing bunch range.

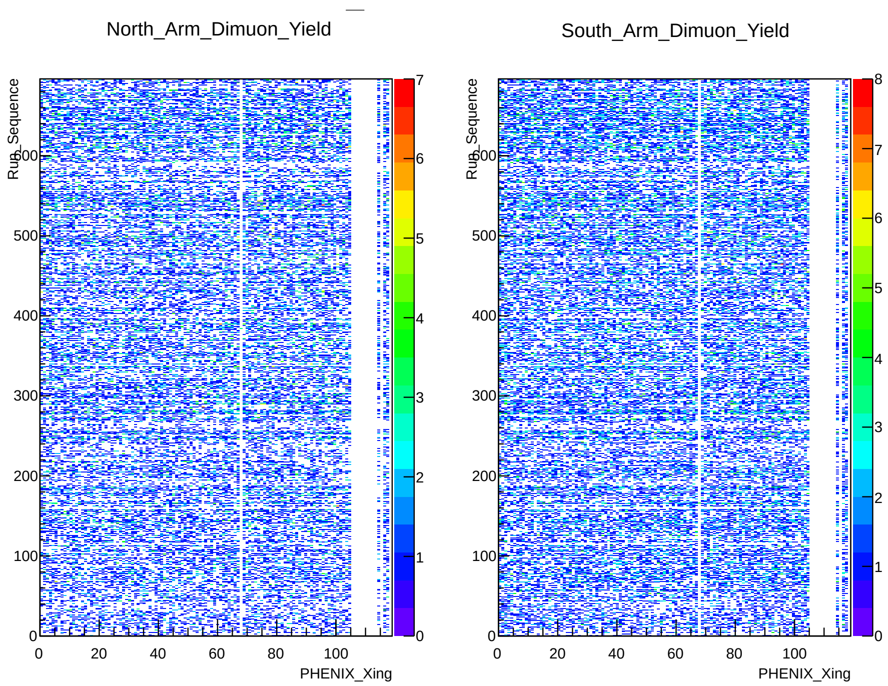

Figure 32: The left plot(North arm) and right plot(South arm) show dimuon yields for each bunch in each run in *pp* collision. Where X axis is PHENIX crossing and Y axis is run sequence

6.1 Crosscheck with Spin Analyzer

Due to the low statistic issue of background in the second x_F bin, the Spin Analyzer is used as a cross check for Maximum Likelihood Method which has been described in last section. The results got from Spin Analyzer are considered as one source of systematic uncertainties.

An overview introduction about Spin Analyzer frame work can be found in Haiwang's analysis note 1194. The most relative features of Spin Analyzer to this analysis are:

1. The spin information is directly loaded from the Spin Database through the standard USpin interface (offline/packages/uspin/). The newest database QA level is used at the time when SpinAnalyzer is run.

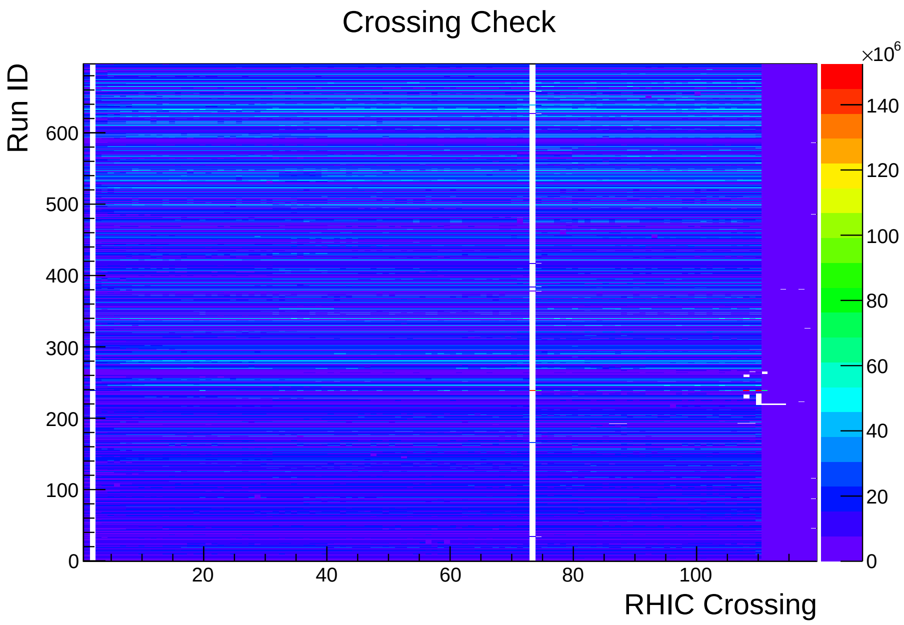

Figure 33: pp BBCin cross check: A 2-D plot filled with BBCin counts reading from Spin Database. X-axis is RHIC crossing and Y-axis is Run sequence

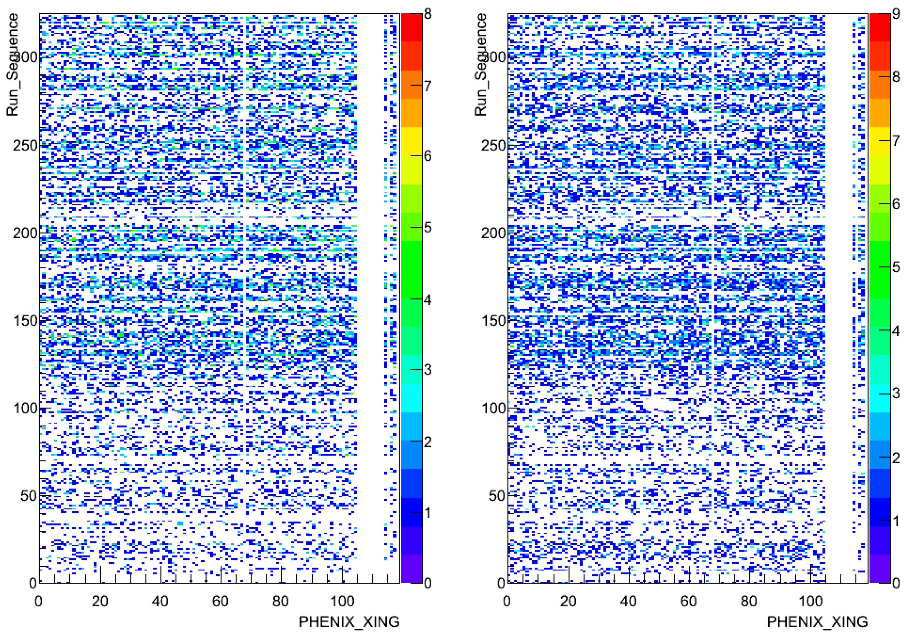

Figure 34: The left plot(North arm) and right plot(South arm) show dimuon yields for each bunch in each run in pAu collision. Where X axis is PHENIX crossing and Y axis is run sequence

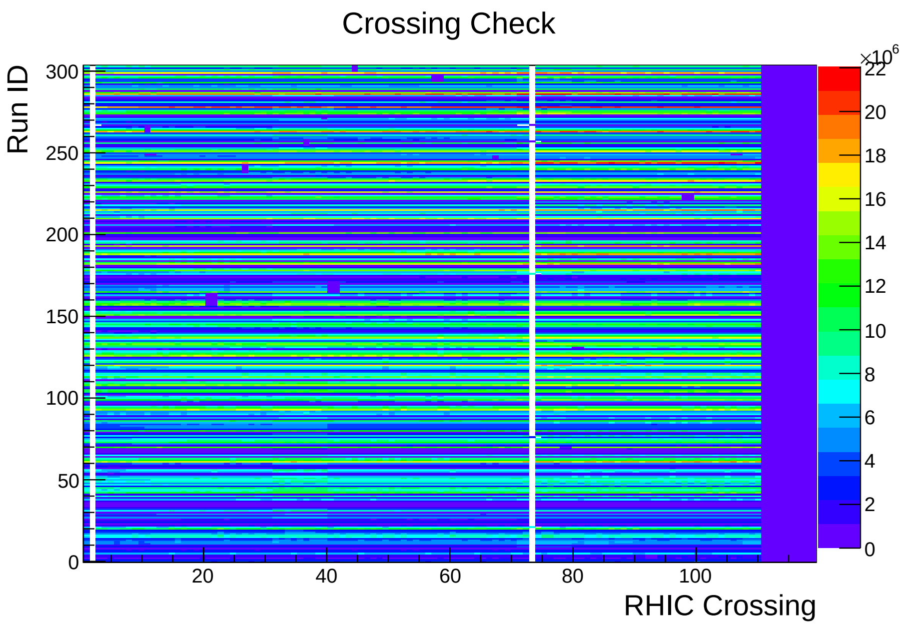

Figure 35: pAu BBCin cross check: A 2-D plot filled with BBCin counts reading from Spin Database. X-axis is RHIC crossing and Y-axis is Run sequence

2. The output from SpinAnalyzer is histograms of counts which is categorized with respect to spin combinations. If chosen, it will also outputs histograms containing the single and double spin-asymmetry results.

3. Haiwang Yu developed a patch to make Spin Analyzer capable to do single polarized beam case such as pAu collision.

6.2 Extract $A_N^{incl(bgr)}$ from Spin Analyzer

Equation 3 shows the definition of A_N as a function of ϕ

$$A_N(\phi) = \frac{\sigma^{\uparrow}(\phi) - \sigma^{\downarrow}(\phi)}{\sigma^{\uparrow}(\phi) + \sigma^{\downarrow}(\phi)} = \frac{1}{P} * \frac{N^{\uparrow}(\phi) - R * N^{\downarrow}(\phi)}{N^{\uparrow}(\phi) + R * N^{\downarrow}(\phi)} \tag{8}$$

Where R is relative luminosity and P is the beam polarization.

For spin = 1/2:

$$\sigma^{\uparrow}(\phi) = \sigma_0 * (1 + A_N * Cos(\phi)) \tag{9}$$

For spin = -1/2:

$$\sigma^{\downarrow}(\phi) = \sigma_0 * (1 - A_N * Cos(\phi)) \tag{10}$$

Insert equation (4) and equation (5) into equation (3), we will get:

$$A_N(\phi) = A_N * Cos(\phi) \tag{11}$$

From Spin Analyzer, $A_N^{incl(bgr)}$ versus ϕ distribution for each p_T bin in both North and South arm will be got automatically after running Spin Analyzer.

For extracting $A_N^{incl(bgr)}$, a cosine modulation fitting function is used and both the value and the uncertainty of $A_N^{incl(bgr)}$ can be extracted from the fitting.

In my analysis, 16 even ϕ bins is set with different p_T bins for both pp and pAu cases. The azimuthal angle ϕ is recorded and calculated under PHENIX coordinate system.

6.3 Spin Analyzer with pp data

6.3.1 Inclusive and Background Asymmetry

The inclusive and background asymmetries extracted from Spin Analyzer are shown from figure 36 to 40. The inclusive asymmetry is calculated from like-sign dimuon within 2σ invariant mass range got from GPR fitting in section 3. The background asymmetry is calculated from the low side band dimuon the mass range of which is from 1.5 to 2.4GeV.

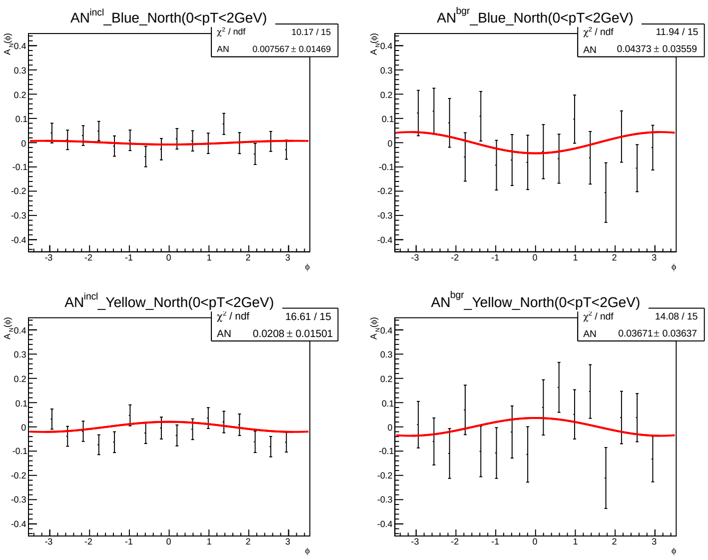

Figure 36: pp Inclusive and background A_N with $0 < p_T < 2GeV$ bin in North arm

6.4 Spin Analyzer with pAu data

In pAu, only proton is polarized and traveling towards positive Z direction so the azimuthal angle is already under PHENIX coordinate system and we can use $\cos(\phi)$ for fitting purpose.

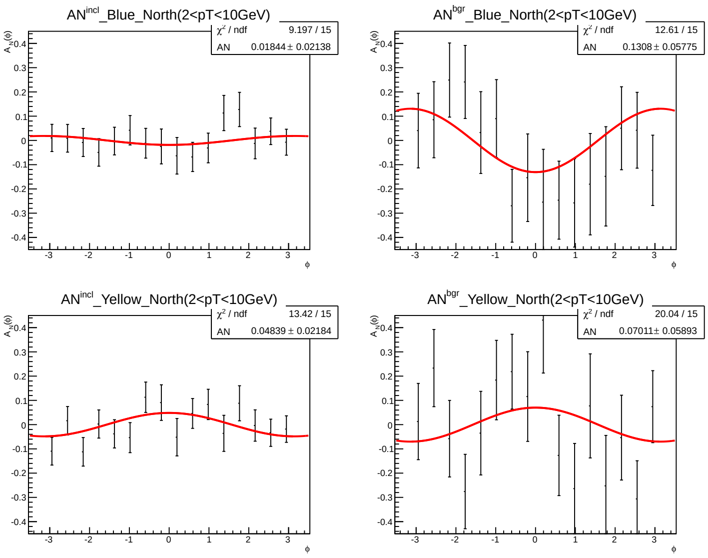

Figure 37: pp Inclusive and background A_N with $2 < p_T < 10GeV$ bin in North arm

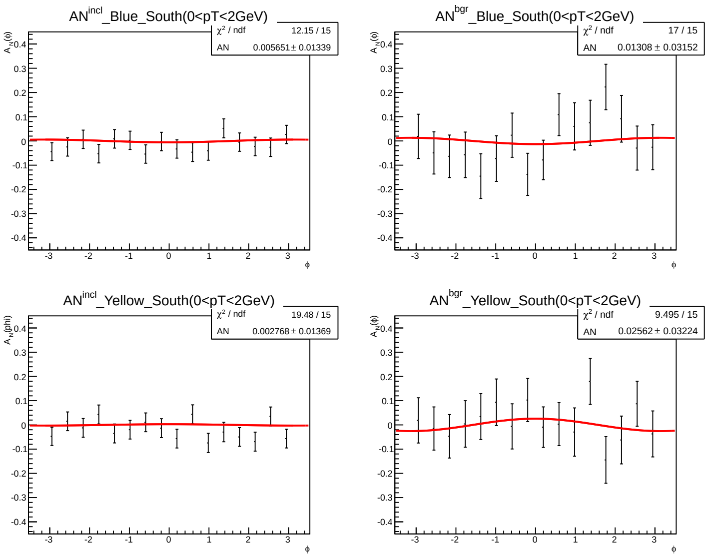

Figure 38: pp Inclusive and background A_N with $0 < p_T < 2GeV$ bin in South arm

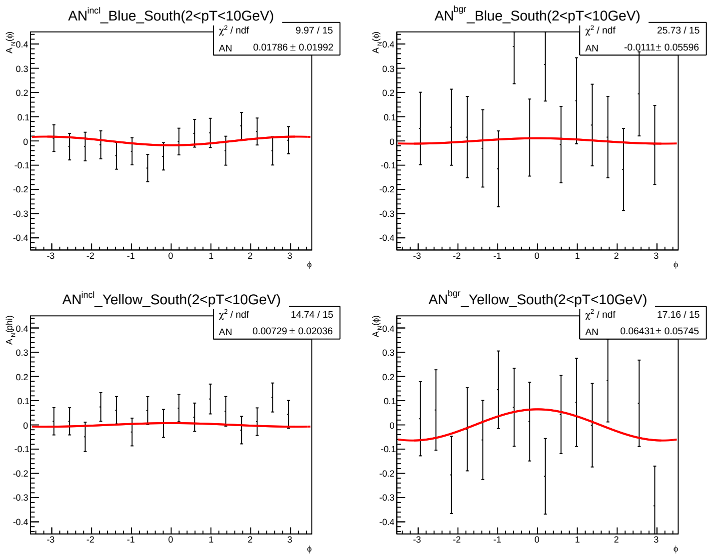

Figure 39: pp Inclusive and background A_N with $2 < p_T < 10GeV$ bin in South arm

6.4.1 Inclusive and background A_N with pAu data after tilt angle correction

Similar with the procedure in pp case, inclusive and background asymmetries with pAu extracted from Spin Analyzer are shown from figure 41 to 44. The inclusive asymmetry is calculated from like-sign dimuon within $2-\sigma$ invariant mass range got from GPR fitting in section 3. The background asymmetry is calculated from the low side band dimuon the mass range of which is from 1.5 to 2.4GeV.

6.5 A crosscheck for Spin Analyzer with standalone code

I also wrote a standalone code to repeat what Spin Analyzer is doing in the background for both pp and pAu analysis. Then compare the result from standalone code with the result from Spin Analyzer.

6.5.1 Cross Check for pp with Standalone code

In pp, since both blue and yellow beam are polarized, equation(3) is rewritten as:

$$A_N(\phi) = \frac{\sigma^{\uparrow\uparrow}(\phi) + \sigma^{\uparrow\downarrow}(\phi) - (\sigma^{\downarrow\uparrow}(\phi) + \sigma^{\downarrow\downarrow}(\phi))}{\sigma^{\uparrow\uparrow}(\phi) + \sigma^{\uparrow\downarrow}(\phi) + \sigma^{\downarrow\uparrow}(\phi) + \sigma^{\downarrow\downarrow}(\phi)} = \frac{1}{P} * \frac{N^{\uparrow\uparrow}(\phi) + R_1 * N^{\uparrow\downarrow}(\phi) - (R_2 * N^{\downarrow\uparrow} + R_3 * N^{\downarrow\downarrow})}{N^{\uparrow\uparrow}(\phi) + R_1 * N^{\uparrow\downarrow}(\phi) - R_2 * N^{\downarrow\uparrow} + R_3 * N^{\downarrow\downarrow}} \quad (12)$$

Where $R_1 = L^{\uparrow\uparrow}/L^{\uparrow\downarrow}$, $R_2 = L^{\uparrow\uparrow}/L^{\downarrow\uparrow}$, $R_3 = L^{\uparrow\uparrow}/L^{\downarrow\downarrow}$.

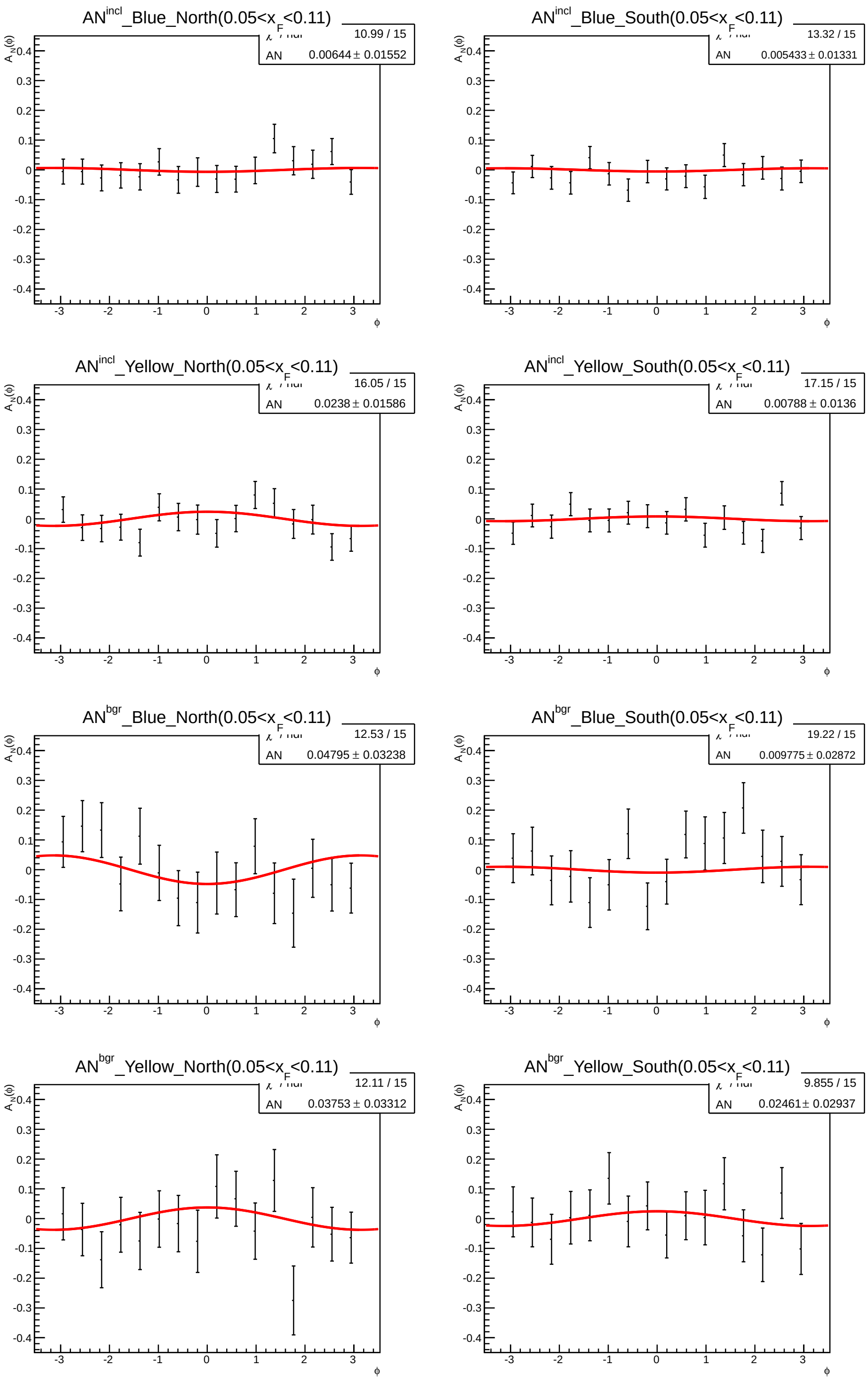

Figure 40: *pp* Inclusive(top plot)&background(bottom plot) A_N with one x_F bin

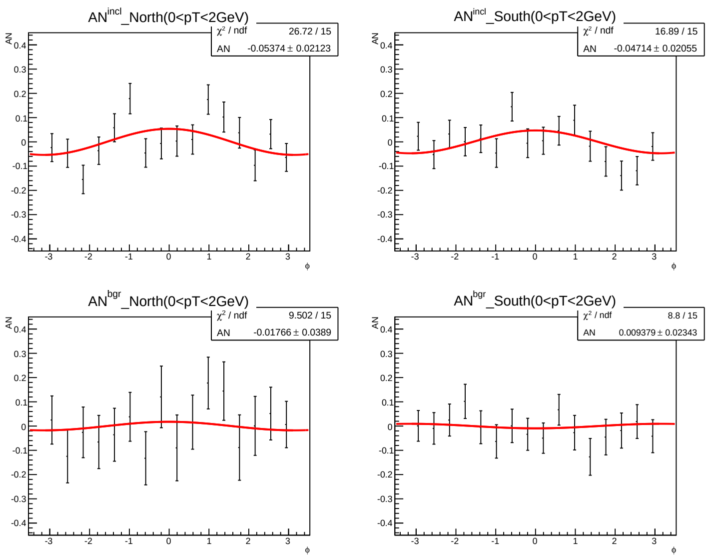

Figure 41: pAu Inclusive and background A_N with $0 < p_T < 2GeV$

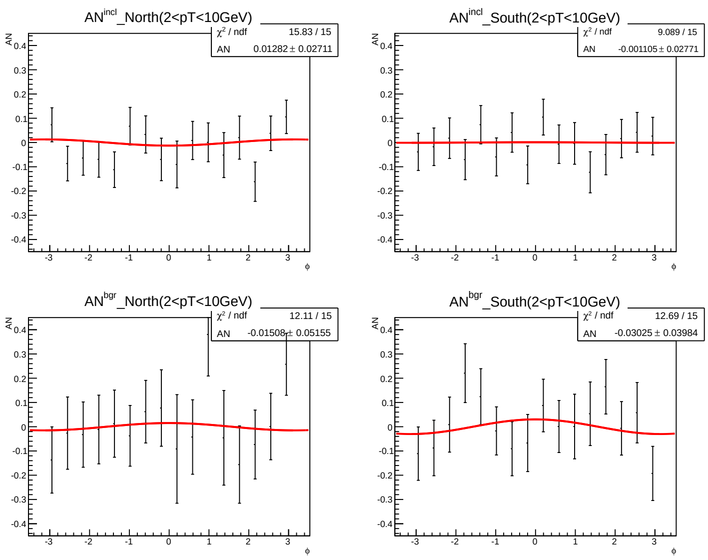

Figure 42: pAu Inclusive and background A_N with $2 < p_T < 10GeV$

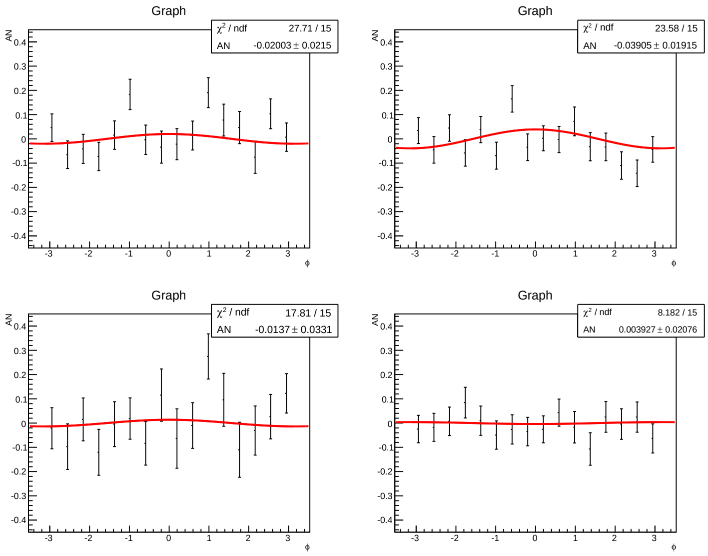

Figure 43: pAu Inclusive and background A_N with $0.05 < x_F < 0.11$

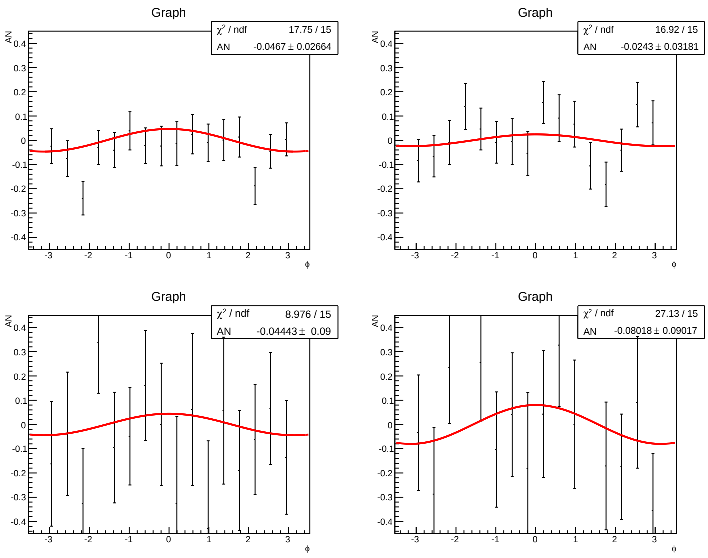

Figure 44: pAu Inclusive and background A_N with $0.11 < x_F < 0.30$

Polarization is the average polarization of all the runs weighted by the run luminosity with $P_{blue} = 57\%$ and $P_{yellow} = 57\%$.

$A_N(\phi)$, relative luminosity(R_1, R_2, R_3) and polarization value for blue and yellow beam got from standalone code are exactly the same with those values calculated by Spin Analyzer.

Figure 45-48 show the inclusive/background A_N fitting result from standalone code. The variance of $A_N^{incl(bgr)}$ with Spin Analyzer and standalone is about 2% σ. This slight discrepancy is due to the different uncertainty calculation for A_N in each ϕ bin. In Spin Analyzer, only number of events are considered into statistical uncertainty while, in standalone code, the polarization is also taken into account.

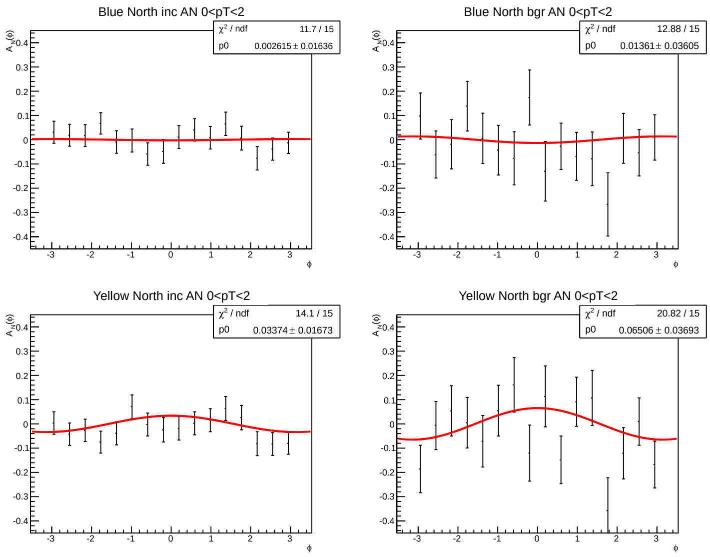

Figure 45: Inclusive and background A_N got from standalone code with $0 < p_T < 2GeV$ bin in North arm with pp data

6.5.2 Cross check for pAu data with standalone code

For pAu collision, only blue beam is polarized. So $A_N^{incl(bgr)}(\phi)$ can be calculated by equation(3). The polarization is the average polarization of all the runs weighted by the run luminosity with $P_{blue} = 60\%$.

Figure 49 to 51 show the inclusive/background A_N in different p_T and x_F bins. An approximately 1%σ shift is observed due to the same reason described in section 7.1.

6.5.3 Fill-by-Fill A_N estimation with Maximum Likelihood method

A fill-by-fill A_N estimation is also covered by Maximum Likelihood method. This is a cross check that whether there is a bias with combined data analysis

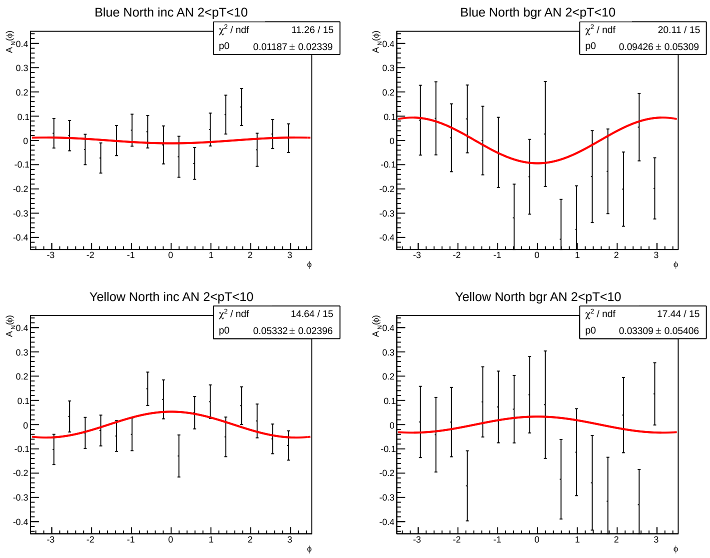

Figure 46: Inclusive and background A_N got from standalone code with $2 < p_T < 10GeV$ bin in North arm with pp data

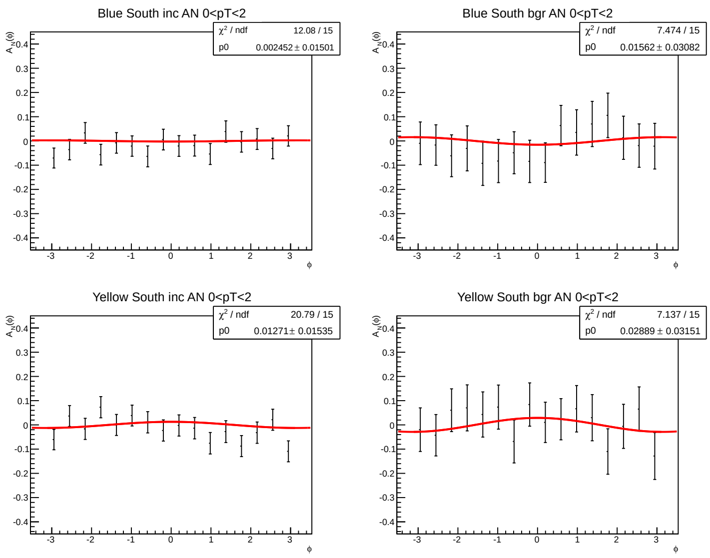

Figure 47: Inclusive and background A_N got from standalone code with $0 < p_T < 2GeV$ bin in South arm with pp data

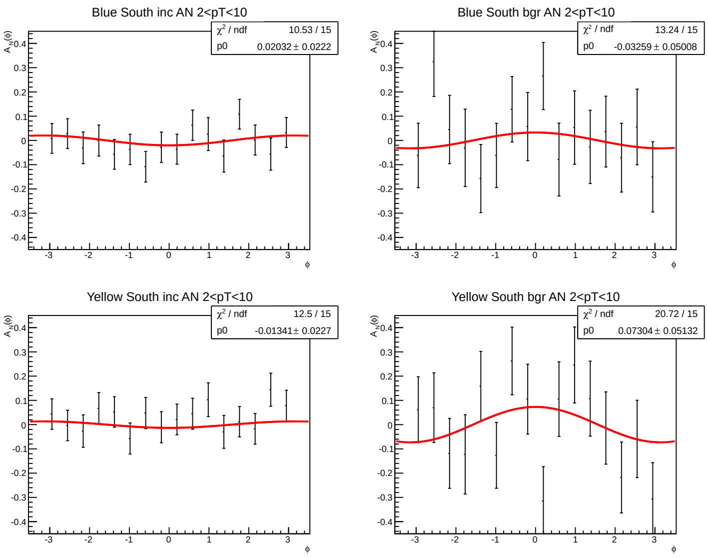

Figure 48: Inclusive and background A_N got from standalone code with $2 < p_T < 10GeV$ bin in South arm with pp data

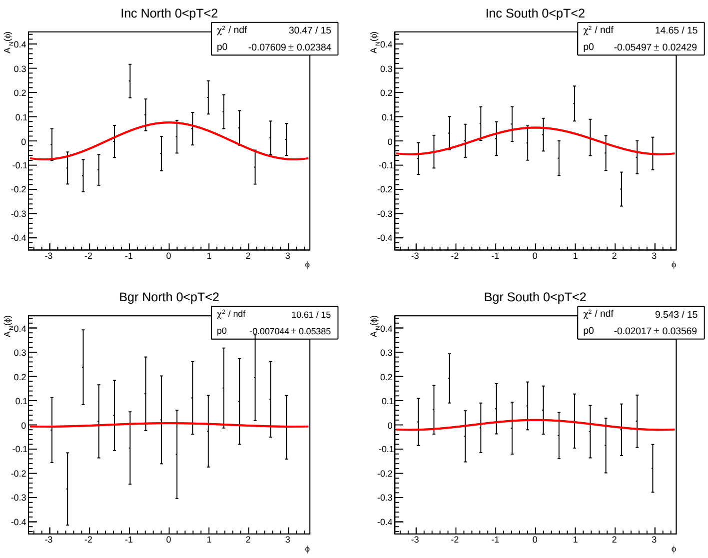

Figure 49: Inclusive and background A_N got from standalone code with $0 < p_T < 2GeV$ with pAu data

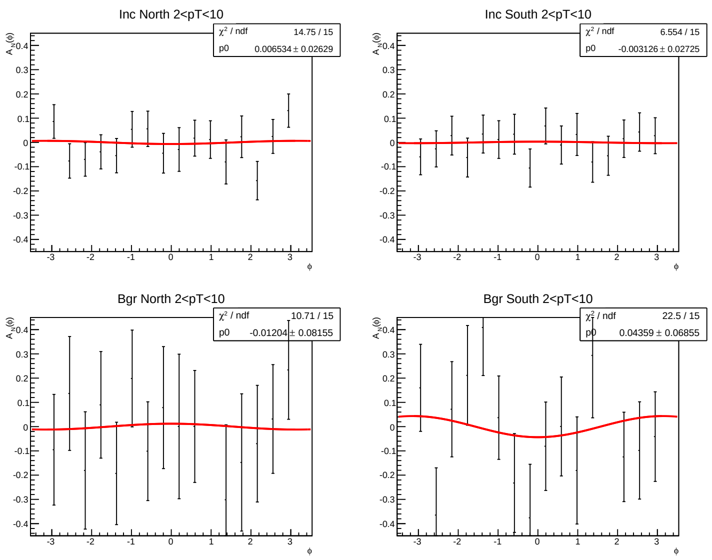

Figure 50: Inclusive and background A_N got from standalone code with $2 < p_T < 10GeV$ with pAu data

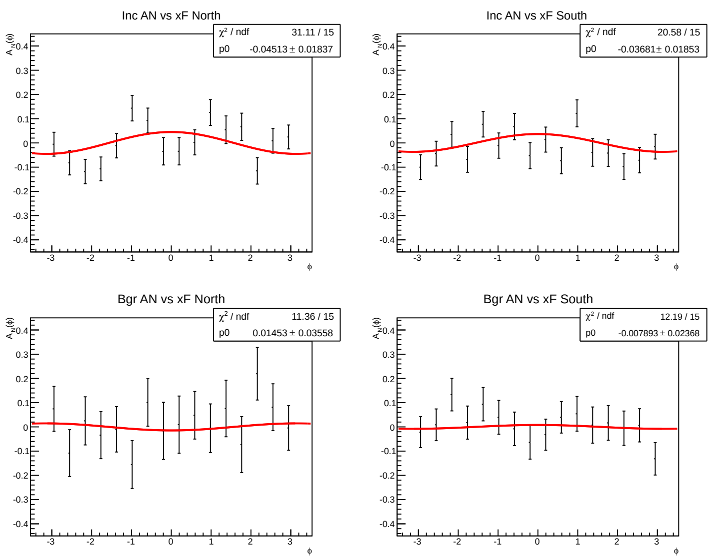

Figure 51: Inclusive and background A_N got from standalone code with one x_F bin with pAu data

which is caused by detector acceptance or/and trigger efficiency change within the whole data taking. Figure 52 shows the Fill-by-Fill result. This result is compared with result got from section 7.7.2. The largest difference observed between this two methods is the inclusive A_N in North arm which varies about 0.15σ difference. Other than that, the difference is all less than 5%. So we may conclude that result with combined data for this analysis is consistent with Fill-by-Fill method.

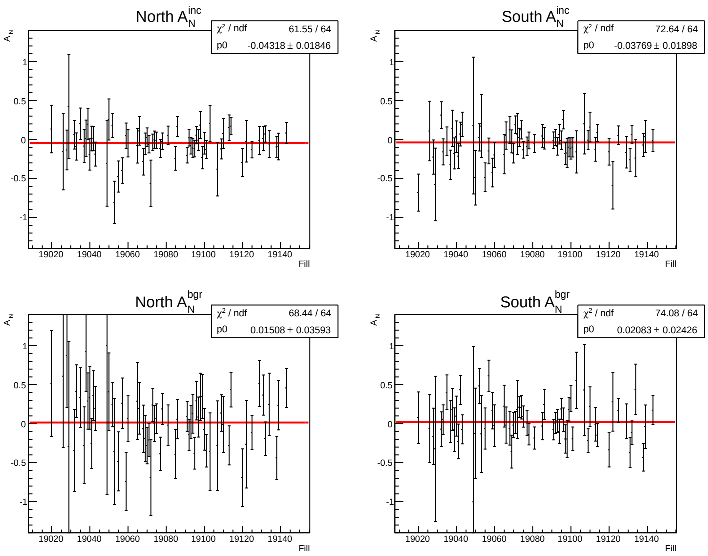

Figure 52: Fill-by-fill Inclusive and background A_N from Maximum Likelihood method with pAu data

6.6 Cross check for pAu data from other collaborators

Another cross check also has been done with Sanghoon and Marie from LANL. I appreciate their time and work on this cross check. A event-by-event check has been performed before comparing the inclusive A_N. In this check, several quantities have been picked for comparison such as x, y, z components of dimuon momentum, azimuthal angle of prompt dimuon and also the spin pattern. And we got perfect match on this part. After that, Sanghoon and I produced inclusive A_N using same picoDST and good run list but different sets of dimuon cuts. Marie was using a different good run list and dimuon cut. The purpose of this cross check is to see whether there is a coding issue. Rather than that, it also check whether we introduced some bias when applying the cut. Figure 53 shows the inclusive A_N for north arm with lower p_T bin. My result is perfectly match with the result produced by Sanghoon. And Marie's result is also consistent with mine. Considering that she was using a different dataset, the fluctuation shown in the figure is expected. With different cut sets, the inclusive A_N is consistent with each other.

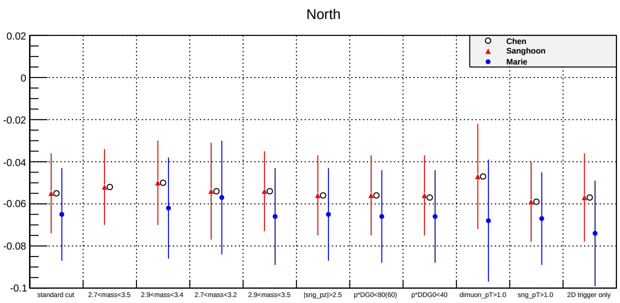

Figure 53: Compare inclusive A_N from different cut set with Sanghoon and Marie using pAu data

7 Discrepancy between preliminary and current result

7.1 Discrepancy due to different taxi production

For preliminary result, we were using production 105. Currently, we are using production 107. The difference between these two productions is the alignment of FVTX. The changing of alignment of FVTX will result in the event vertex shift which will affect the refitting in the dimuon reconstruction process. For the MuTr tracks that match with FVTX tracklets, the mass and momentum will change about 1% due to the alignment. The change of mass and momentum will shift the final result by about 0.2 sigma as we can see in figure 54.

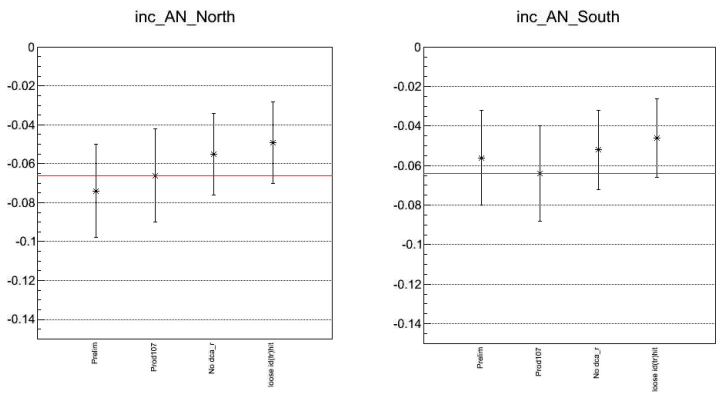

Figure 54: Compare inclusive A_N from different production and cut with pAu data. The x-axis is

7.2 Discrepancy due to different single muon dca_r cut

Single muon dca_r is filled into picoDST with the strategy in following: if the track of single muon from Mutr match with the tracklet from FVTX, fill Mutr dca_r with FVTX dca_r into picoDST. Otherwise, fill single muon container with

Mutr dca_r. Previous dca_r cut at 5 is applied on both FVTX and MuTr dca_r. Now all the dca_r is calculated with the Mutr dca_r definition. The dca_r cut is applied at 10 in order to keep as many statistics as possible and also minimize the hadronic in background mass region. Figure 55 shows Mutr dca_r distribution in north and south arm with pAu data.

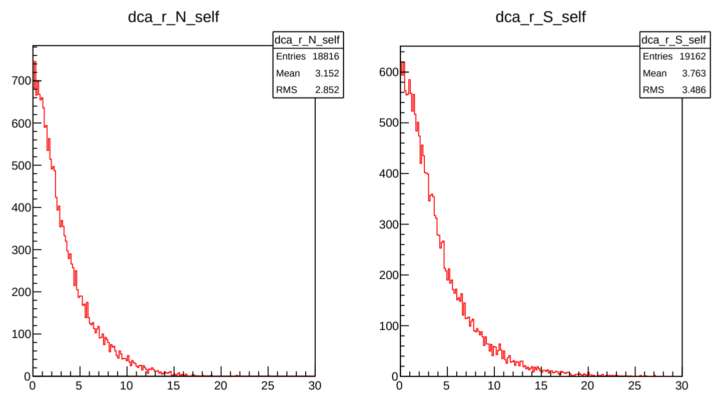

Figure 55: Top: Single muon dca_r distribution from FVTX. Bottom: Single muon dca_r distribution from Mutr.

8 Further study for A_N in first p_T bin with pAu data

As it has been shown in section 5, we observed a negative 2.5-sigma level A_N in first p_T bin with pAu data. In order to find the possible reason for causing it, we checked the A_N with different subsystem activities, such as number of FVTXTracklets and BBC centrality(BBC charge).
Studying on different subsystem activities means more binning will be made for the first p_T bin. In other words, the statistics for low side band will be too low to carry a good analysis for background A_N. However, inclusive A_N would be good enough for this study since dimuons are dominant(90%) in 2-sigma dimuon mass window.

8.1 A_N with number of FVTXTracklets

For each dimuon that passed the dimuon event cuts, the corresponding number of FVTXTracklets information will be calculated with the data collected by FVTX. A total number of FVTXTracklets is already in picoDST. The FVTX-Tracklets which is coming from dimuons or with less than two hits in FVTX or FVTX dca_r ¿ 1.0 will be excluded from total number of FVTXTracklets. Figure 56 shows the number of FVTXTracklets distribution. Basing on the distribution, four bins has been made for number of FVTXTracklets. Each bin has roughly equal statistics.

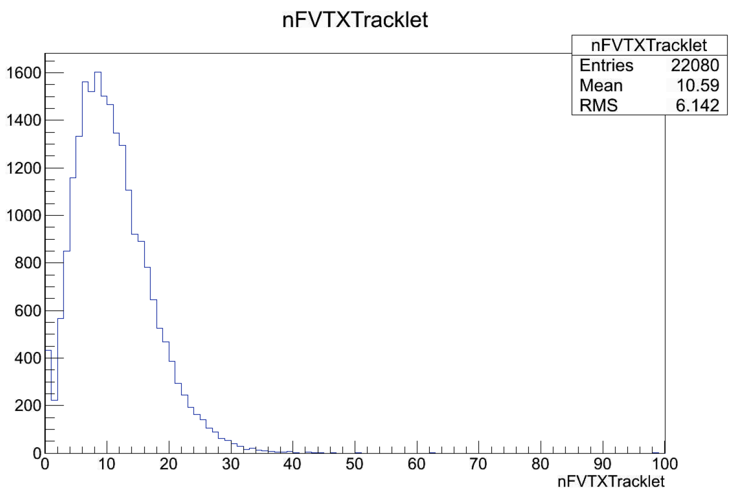

Figure 56: FVTX Tracklets distribution for the dimuons that pass the dimuon event cuts with pAu data

Figure 57 shows the inclusive A_N in each number of FVTXTracklets bin.

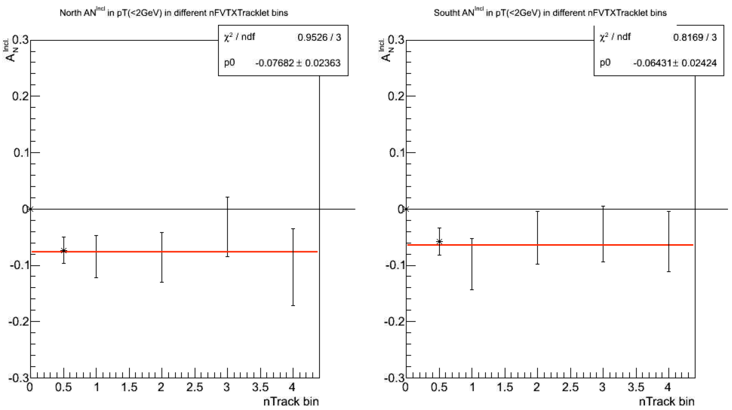

Figure 57: Inclusive A_N vs. nFVTXTracklets. The first point(star point) is the combined inclusive A_N for first p_T bin got in section 6.

8.2 A_N with BBC centrality(charge)

Similar with number of FVTXTracklets, BBC centrality distribution is got for the dimuons that pass the dimuon event cuts. Figure 58 is BBC centrality distribution. Basing on the distribution, four bins has been made for BBC centrality. Each bin has roughly equal statistics.

Figure 59 is inclusive A_N in each BBC centrality(charge) bin. Considering that higher BBC centrality is corresponding to lower BBC charge, the BBC

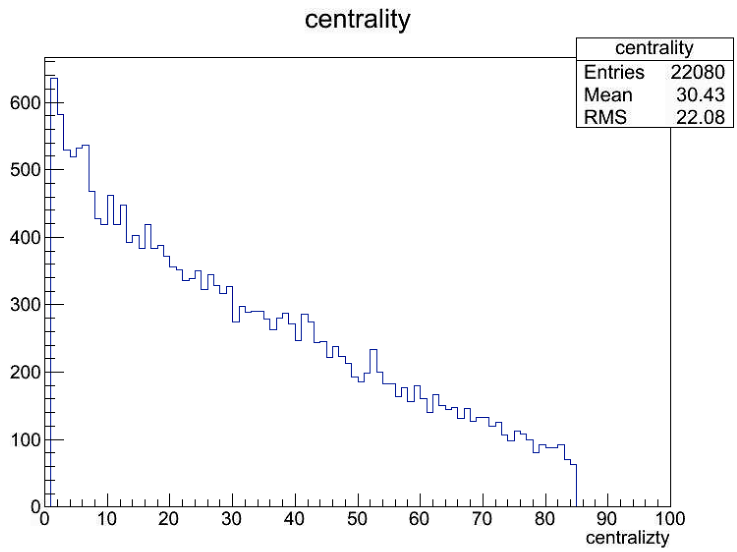

Figure 58: BBC centrality distribution for the dimuons that pass the dimuon event cuts with pAu data

centrality binning in the figure is in the descending order.

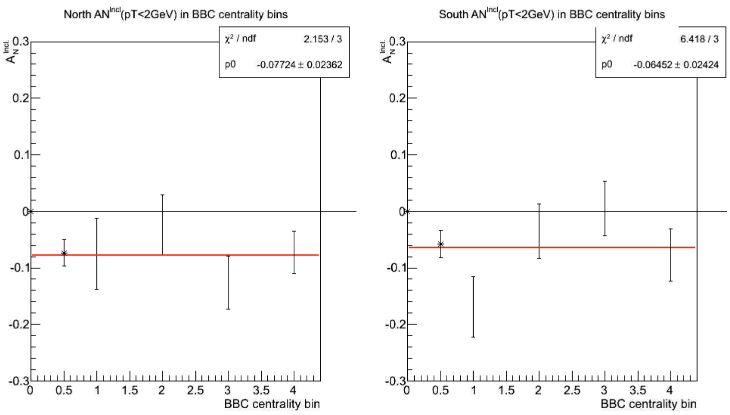

Figure 59: Inclusive A_N vs. BBC centrality. The first point(star point) is the combined inclusive A_N for first p_T bin got in section 6.

8.3 A_N in three and four p_T bins

In order to check whether there exist a p_T dependent A_N, it would be helpful to make the number of p_T bin three and four rather than just two. Figure 60 and figure 61 show the inclusive A_N in three and four p_T bins. In the case of three p_T bins, the binning is [0GeV,1.2GeV],[1.2GeV,2GeV] and [2GeV,10GeV]. While in the case of four p_T bins, the binning is [0GeV,1.GeV], [1.GeV,1.8GeV], [1.8GeV,2.8GeV]and [2.8GeV,10GeV].

Since pAu data is very limited, the inclusive A_N with further binning in nFVTXTracklets and centrality is consistent with each other with relatively big statistical uncertainty. We cannot find out very strong evidences to show that A_N is dependent on nFVTXTracklets or/and centrality.

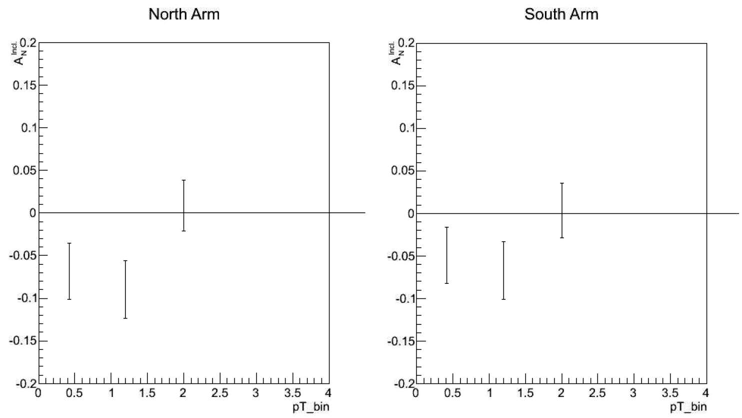

Figure 60: Inclusive A_N with three p_T bins.

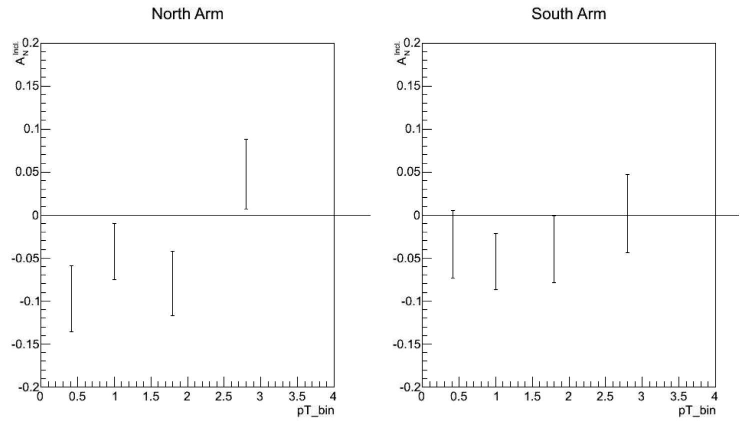

Figure 61: Inclusive A_N with four p_T bins.

9 Systematic Uncertainty Study

In this section the results of a number of systematic studies are presented where the stability of the result is being probed.

9.1 Bunch shuffling result for transverse single spin A_N

Shuffling the assigned spin direction for each bunch is a method to check for bunch related false asymmetries. Those can occur if the acceptance or efficiency of the trigger or the detector depend on the bunch structure or the timing. By definition the average asymmetries with randomized spins are zero, but the distribution of asymmetries from many randomized samples would be wider than expected. Bunch shuffling is not sensitive to any physics related asymmetry, i.e., an asymmetry of the MiniBias trigger physics itself, background asymmetries or trigger biases. Of course, bunch shuffling is only sensitive to effects of a similar magnitude as the statistical error of the asymmetry.

The systematic bias has been checked with bunch shuffling. The procedure is:

1. randomly reassign the polarization direction for each bunch crossing,
2. recalculate the asymmetry,
3. repeat many times(in our case is 10000) to produce a shuffled asymmetry distribution centered around zero,
4. compare width of shuffled distribution to statistical error on the physics asymmetry

Figure 62 and 63 show the bunch shuffling result for pp in two p_T and figure 64 and 65 show the bunch shuffling result for p(Au). Those plots show that the peak of the Gaussian distribution is around zero and σ is around one.

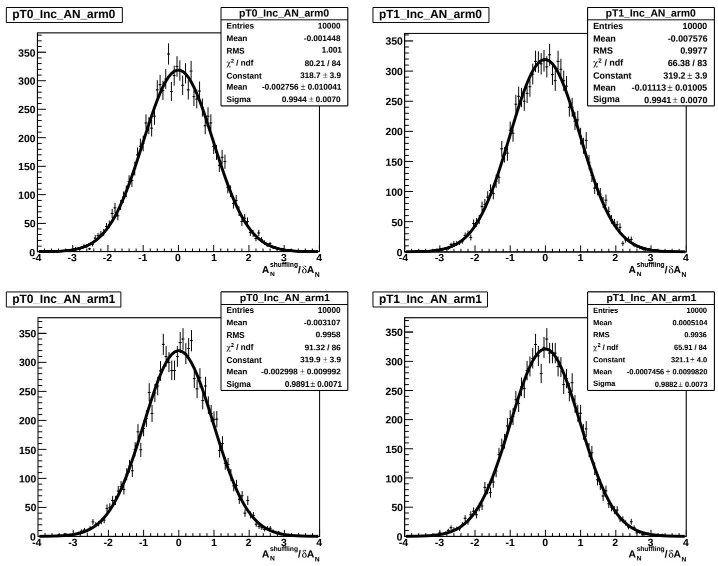

Figure 62: 10000 times bunch shuffling p_T dependent inclusive asymmetries calculated by standalone code on blue beam with pp data

9.2 Systematic uncertainty from different invariant mass fitting

The other source of systematic uncertainty comes from background fraction got from different fitting methods. The dimuon invariant mass is fitted by one

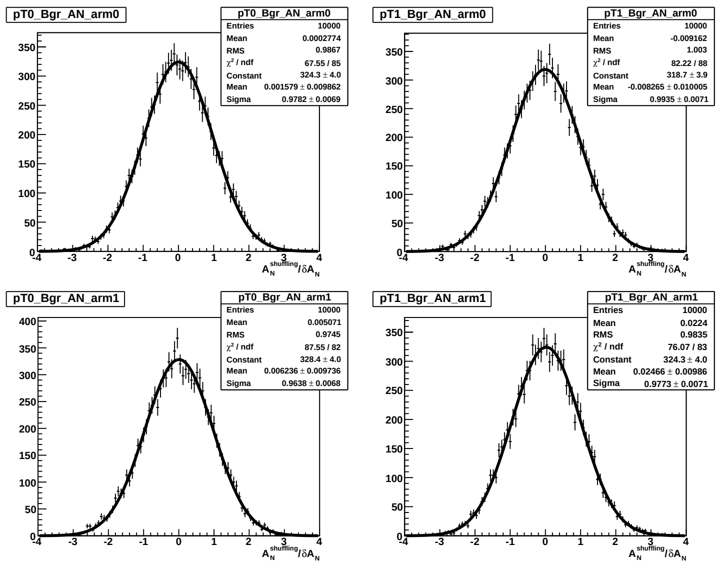

Figure 63: 10000 times bunch shuffling p_T dependent background asymmetries calculated by standalone code on blue beam with pp data

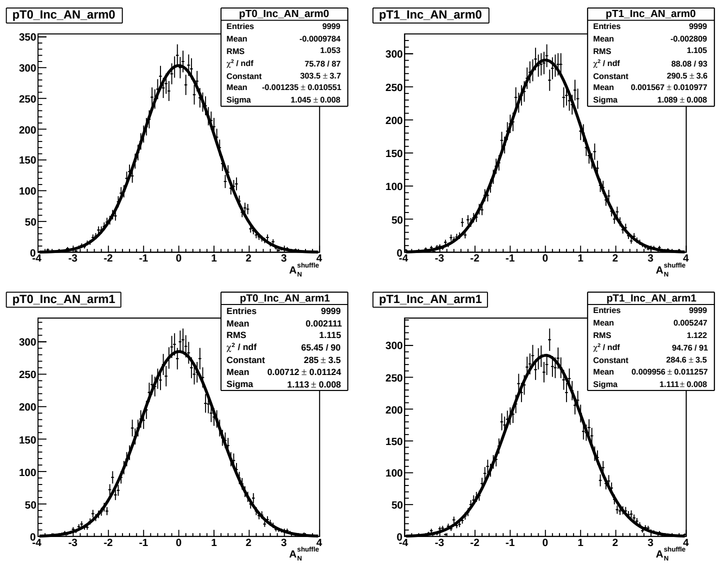

Figure 64: 10000 times bunch shuffling p_T dependent inclusive asymmetries calculated by standalone code on blue beam with pAu data

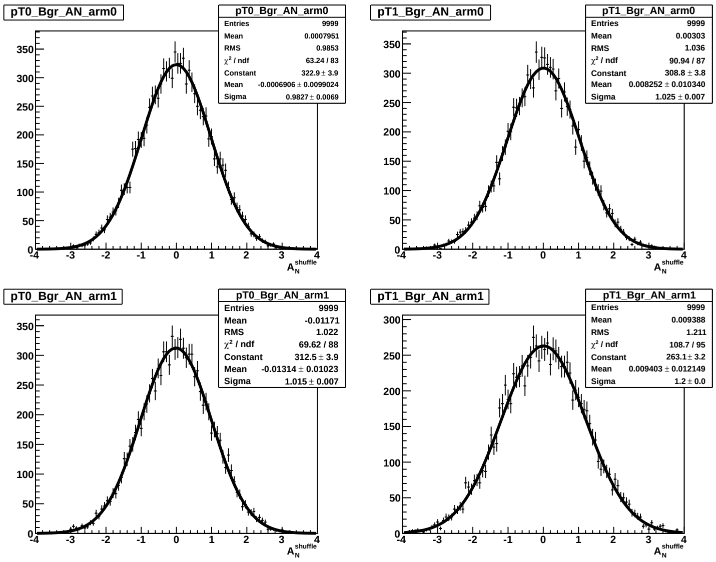

Figure 65: 10000 times bunch shuffling p_T dependent background asymmetries calculated by standalone code on blue beam with pAu data

Crystal Ball function for J/ψ peak, one Gaussian function for ψ' peak and a third-order polynomial for the background.

The fitting result with pp data is shown in figure 66 to 68 and figure 69 to 74 show the fitting result with pAl and pAu data respectively.

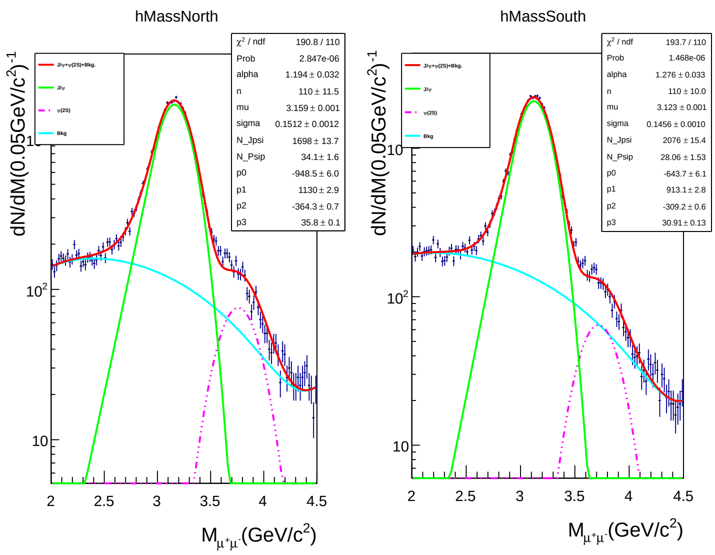

Figure 66: CB+Gaussian+Pol3 fitting in North and South arm with pp data

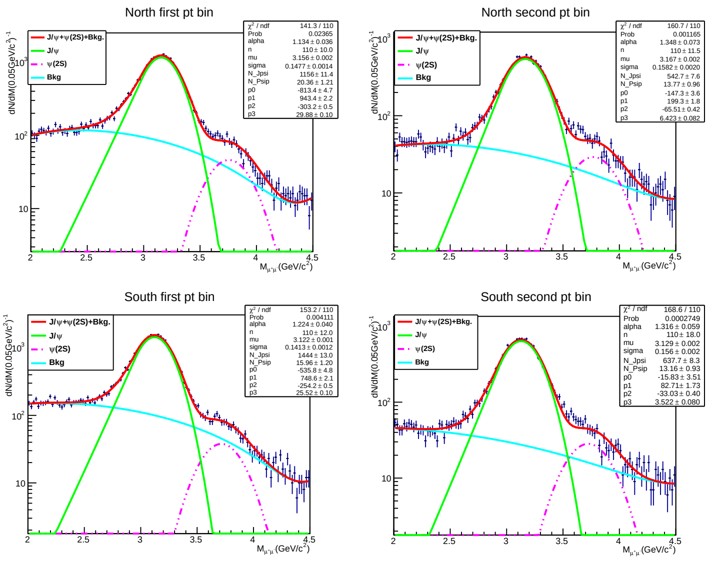

Figure 67: CB+Gaussian+Pol3 fitting in North and South arm for different p_T bins with pp data

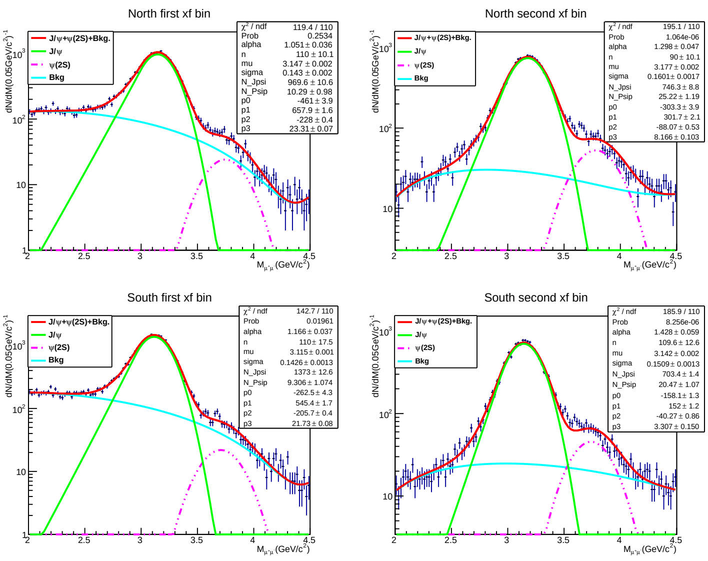

Figure 68: CB+Gaussian+Pol3 fitting in North and South arm for different x_F bins with pp data

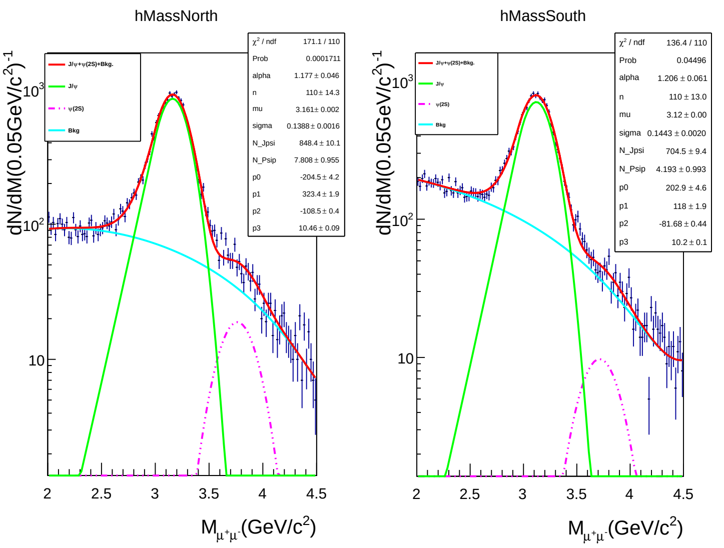

Figure 69: CB+Gaussian+Pol3 fitting in North and South arm with pAu data

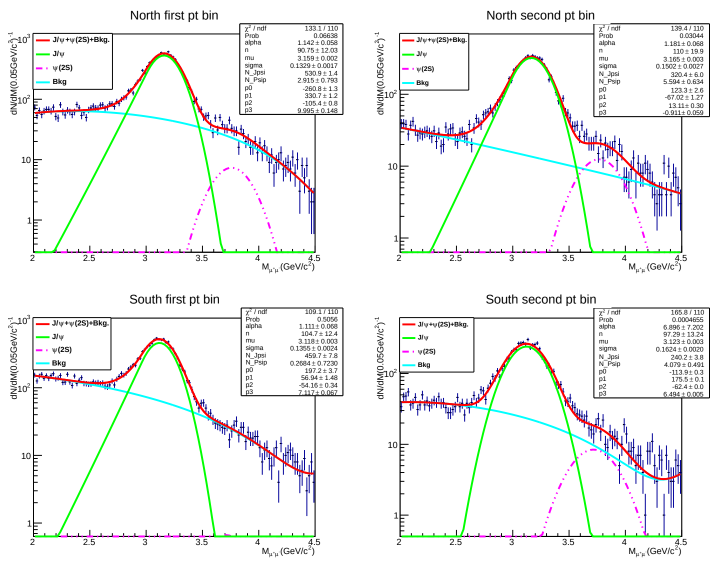

Figure 70: CB+Gaussian+Pol3 fitting in North and South arm for different p_T bins with pAu data

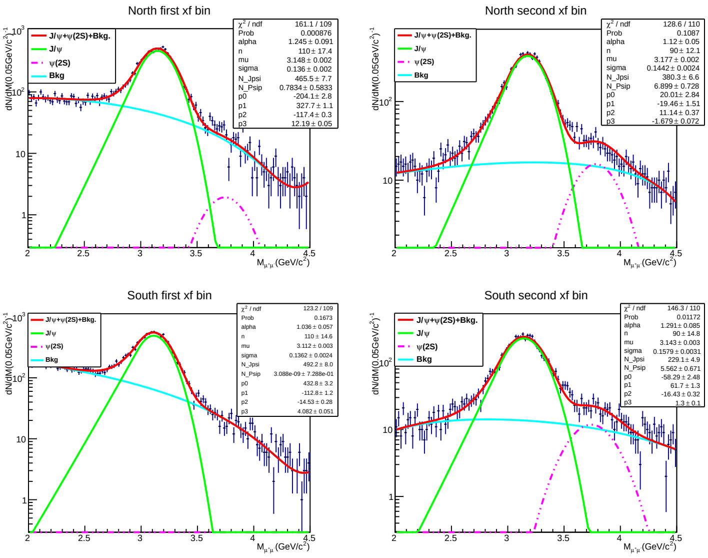

Figure 71: CB+Gaussian+Pol3 fitting in North and South arm for different x_F bins with pAu data

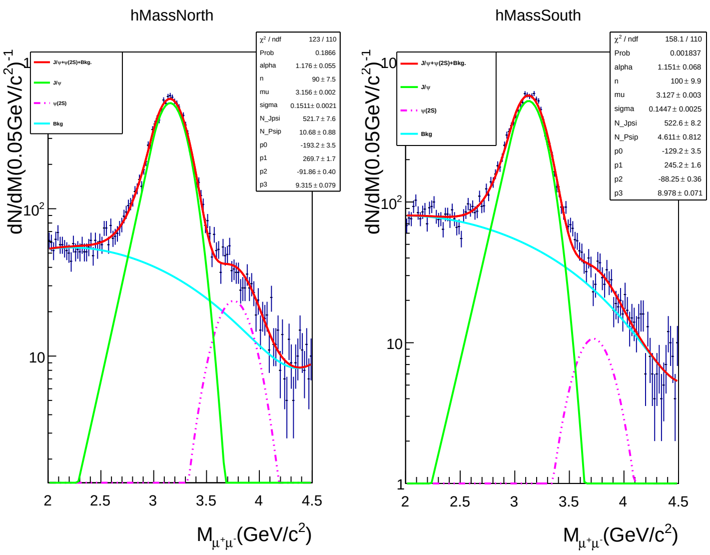

Figure 72: CB+Gaussian+Pol3 fitting in North and South arm with pAl data

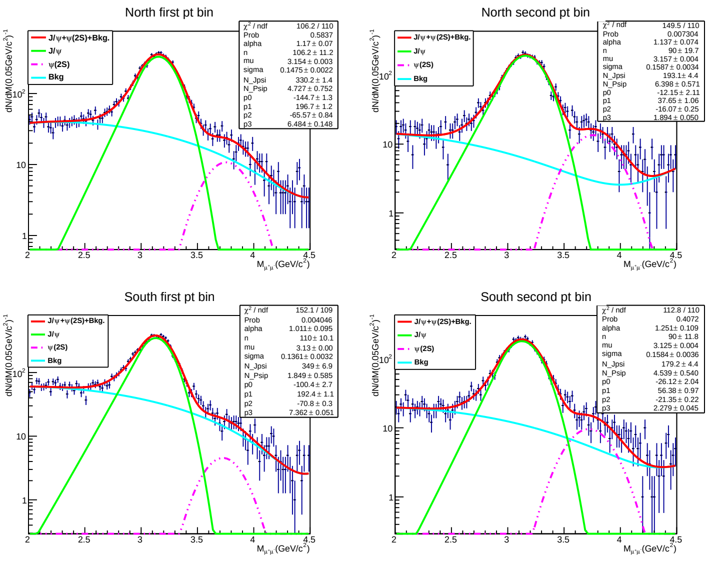

Figure 73: CB+Gaussian+Pol3 fitting in North and South arm for different p_T bins with pAl data

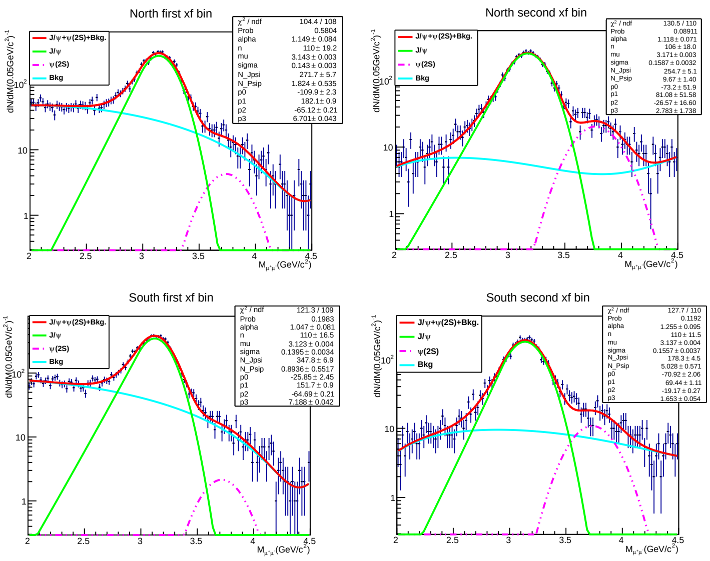

Figure 74: CB+Gaussian+Pol3 fitting in North and South arm for different x_F bins with pAl data

A set of background fraction is got using this new fitting function with pp, pAl and pAu data. Table 17, 18 and 19 list the background fraction for each bin. The differences between two different fitting methods in each bin are treated as systematic uncertainty of background fraction and it propagates to the systematic uncertainty of $A_N^{J/\psi}$ using equation:

$$\delta_{sys} A_N^{J/\psi} = \frac{\partial A_N^{J/\psi}}{\partial f} \dot{\delta f} = \frac{A_N^{Incl.} - A_N^{bgr}}{(1-f)^2} \dot{\delta f} \tag{13}$$

p_T	$f_{Bgr} \pm \delta f_{Bgr}(Stat.)(\%)$ North	$f_{Bgr} \pm \delta f_{Bgr}(Stat.)(\%)$ South
$p_T \in 0-2$	11.6	10.7
$p_T \in 2-10$	9.0	8.2
$x_F \in 0.05-0.11$	12.8	11.4
$x_F \in 0.11-0.30$	6.4	5.7

Table 17: Background Fraction with CB + Gaussian + 3Pol for pp data

p_T	$f_{Bgr} \pm \delta f_{Bgr}(Stat.)(\%)$ North	$f_{Bgr} \pm \delta f_{Bgr}(Stat.)(\%)$ South
$p_T \in 0-2$	12.7	18.7
$p_T \in 2-10$	10.9	10.5
$x_F \in 0.05-0.11$	13.5	18.1
$x_F \in 0.11-0.30$	7.2	8.9

Table 18: Background Fraction with CB + Gaussian + 3Pol for pAu data

p_T	$f_{Bgr} \pm \delta f_{Bgr}(Stat.)(\%)$ North	$f_{Bgr} \pm \delta f_{Bgr}(Stat.)(\%)$ South
$p_T \in 0-2$	11.9	13.8
$p_T \in 2-10$	7.1	8.9
$x_F \in 0.05-0.11$	13.4	14.3
$x_F \in 0.11-0.30$	3.5	7.2

Table 19: Background Fraction with CB + Gaussian + 3Pol for pAl data

9.3 Systematic Uncertainty from A_N^{bgr} in different mass window

As it has been described in previous section, A_N^{bgr} is estimated using the low side band dimuon mass range which is from 1.5GeV to 2.4GeV. Two different mass windows are used for estimating A_N^{bgr}: 1.3GeV - 1.9GeV and 1.9GeV - 2.5GeV. We use A_N^{bgr} from 1.9GeV - 2.5GeV mass window to calculate the systematic uncertainty in this analysis. Figure 75 to 77 show the A_N^{bgr} in p_T bins got from different low side band mass range. The differences of $A_N^{J/\psi}$ got from those A_N^{bgr} are treated as one of the systematic uncertainty sources.

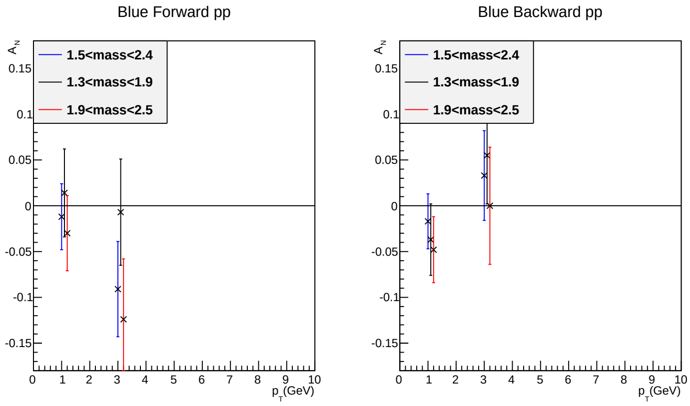

Figure 75: A_N^{bgr} in p_T bins on Blue beam with different low side mass windows with pp data

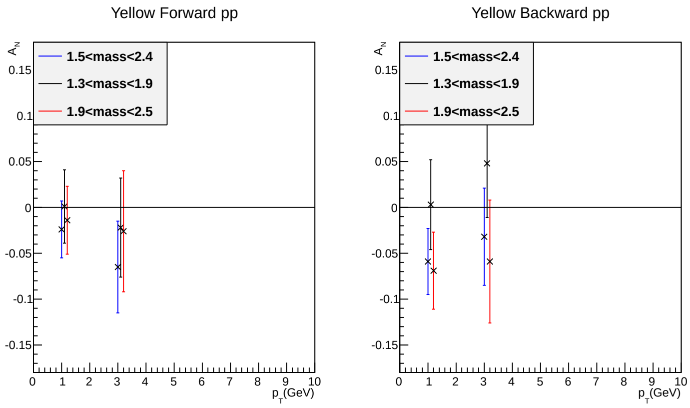

Figure 76: A_N^{bgr} in p_T bins on Yellow beam with different low side mass windows with pp data

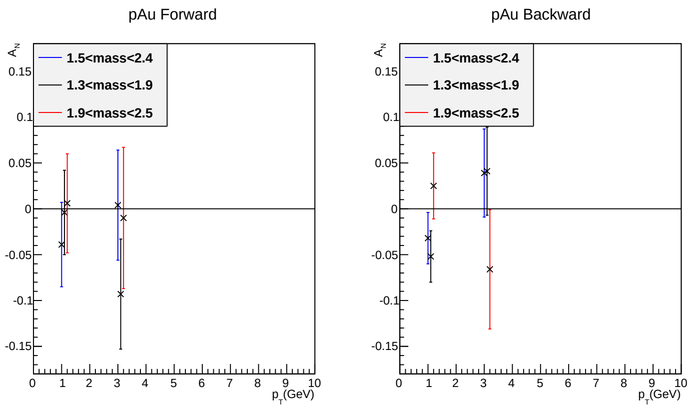

Figure 77: A_N^{bgr} in p_T bins with different low side mass windows with pAu data

9.4 Combining Systematic Uncertainty from different sources

So far, three sources of systematic uncertainty are discussed in previous section. Source one is the systematic uncertainty coming from using different analysis method as we described in section 7. The other systematic uncertainty source is related with background fraction with different fitting methods. The last one is from A_N^{bgr} estimated with different mass windows. These sources are independent with each other. Therefore, they can be combined together by using function:

$$\delta_{sys.}A_N = \sqrt{\delta^2_{sys.(ML)}A_N + \delta^2_{sys.(fit)}A_N + \delta^2_{sys.(bgr)}A_N} \quad (14)$$

10 Summary And Final Result

The transverse single spin asymmetries A_N in prompt muons productions (mostly from open heavy flavor decays) are measured as a function of x_F (one bin) and p_T (two bins) by using Run15 data.

For *pp* collision, since both proton beams are porlarized, we need to combine blue beam with yellow beam for forward and backward A_N using equation 13:

$$A_N^{comb.} = \frac{A_N^{Blue} \cdot 1/(\delta_{stat.}A_N^{Blue})^2 + A_N^{Yellow} \cdot 1/(\delta_{stat.}A_N^{Yellow})^2}{1/\delta^2_{stat.}A_N^{Blue} + 1/\delta^2_{stat.}A_N^{Yellow}} \quad (15)$$

The statistic uncertainty is given by:

$$\delta^2_{stat.}A_N^{comb.} = \frac{1}{1/\delta^2_{stat.}A_N^{Blue} +_{stat.} 1/\delta^2 A_N^{Yellow}} \quad (16)$$

The systematic uncertainty from background fraction is given by:

$$\delta_{sys.}A_N^{comb.} = \sqrt{(\frac{\partial A_N^{comb.}}{\partial A_N^{Blue}})^2 \delta^2_{sys.}\dot{A}_N^{Blue} + (\frac{\partial A_N^{comb.}}{\partial A_N^{Yellow}})^2 \delta^2_{sys.}\dot{A}_N^{Yellow}} \quad (17)$$

Figure 78 and 79 show the $A_N^{J/\psi}$ with statistic and combined systematic uncertainty and table 20, 21 and 22 list the value of $A_N^{J/\psi}$ as well as systematic /statistical uncertainties in each bin for *pp*, *p*Al and *p*Au data. Figure 80 shows the comparison between Run15 and previous analysis result. The fluctuation for each point is about 1 sigma.

	North Arm	South Arm
p_T	$A_N^{J/\psi} \pm \delta A_N^{J/\psi}(Stat.) \pm \delta A_N^{J/\psi}(Syst.)$	$A_N^{J/\psi} \pm \delta A_N^{J/\psi}(Stat.) \pm \delta A_N^{J/\psi}(Syst.)$
$p_T \in 0-2$	$0.004 \pm 0.011 \pm 0.003$	$0.013 \pm 0.011 \pm 0.002$
$p_T \in 2-10$	$0.004 \pm 0.015 \pm 0.004$	$0.032 \pm 0.016 \pm 0.003$
$x_F \in 0.05-0.11$	$0.004 \pm 0.011 \pm 0.001$	$0.014 \pm 0.011 \pm 0.003$
$x_F \in 0.11-0.30$	$0.001 \pm 0.015 \pm 0.004$	$0.030 \pm 0.015 \pm 0.003$

Table 20: $A_N^{J/\psi}$ with systematic uncertainty in different p_T bins with *pp* data

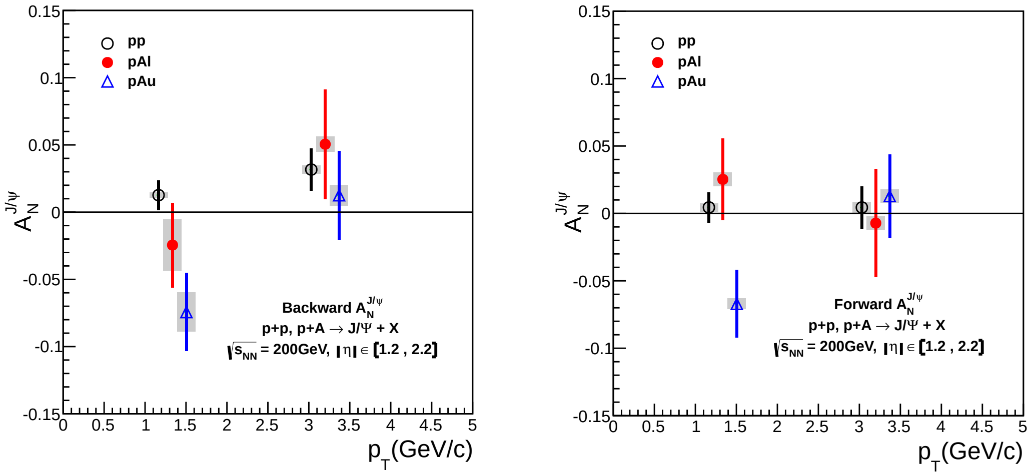

Figure 78: Forward and Backward $A_N^{J/\psi}$ in different p_T bins with pp, pAl and pAu data

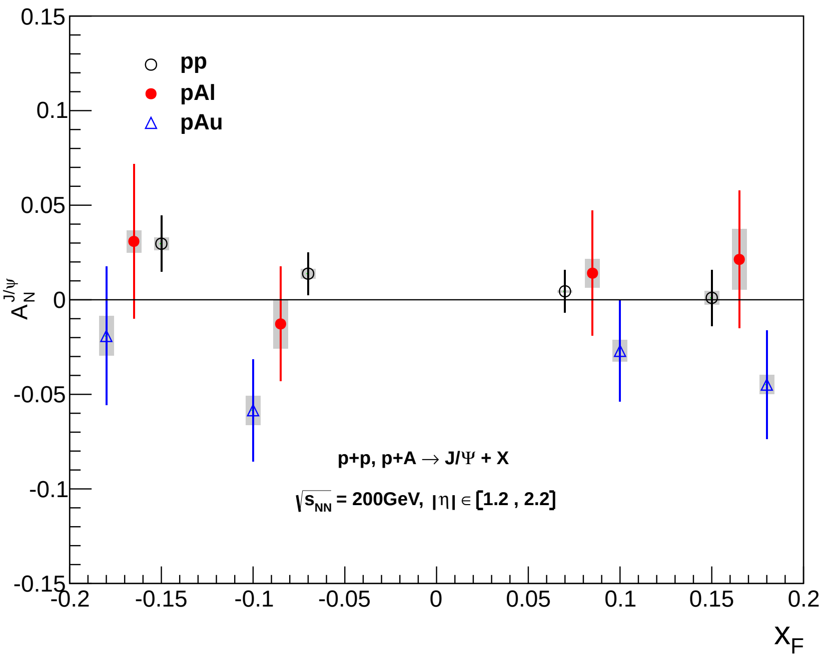

Figure 79: $A_N^{J/\psi}$ in all x_F with pp, pAl and pAu data

p_T	North Arm $A_N^{J/\psi} \pm \delta A_N^{J/\psi}(Stat.) \pm \delta A_N^{J/\psi}(Syst.)$	South Arm $A_N^{J/\psi} \pm \delta A_N^{J/\psi}(Stat.) \pm \delta A_N^{J/\psi}(Syst.)$
$p_T \in 0-2$	0.025± 0.030 ± 0.005	-0.024 ± 0.032 ± 0.019
$p_T \in 2-10$	-0.011 ± 0.039 ± 0.005	0.050 ± 0.041 ± 0.006
$x_F \in 0.05-0.11$	0.014 ± 0.033 ± 0.016	-0.013 ± 0.030 ± 0.013
$x_F \in 0.11-0.30$	0.021± 0.036 ± 0.008	0.031 ± 0.041 ± 0.006

Table 21: $A_N^{J/\psi}$ with systematic uncertainty in different p_T bins with pAl data

p_T	North Arm $A_N^{J/\psi} \pm \delta A_N^{J/\psi}(Stat.) \pm \delta A_N^{J/\psi}(Syst.)$	South Arm $A_N^{J/\psi} \pm \delta A_N^{J/\psi}(Stat.) \pm \delta A_N^{J/\psi}(Syst.)$
$p_T \in 0-2$	-0.067 ± 0.025 ± 0.004	-0.074 ± 0.029 ± 0.014
$p_T \in 2-10$	0.013 ± 0.031 ± 0.005	0.012 ± 0.033 ± 0.008
$x_F \in 0.05-0.11$	-0.027± 0.027 ± 0.006	-0.058 ± 0.027 ± 0.008
$x_F \in 0.11-0.30$	-0.045 ± 0.029 ± 0.005	-0.019± 0.037 ± 0.011

Table 22: $A_N^{J/\psi}$ with systematic uncertainty in different p_T bins with pAu data

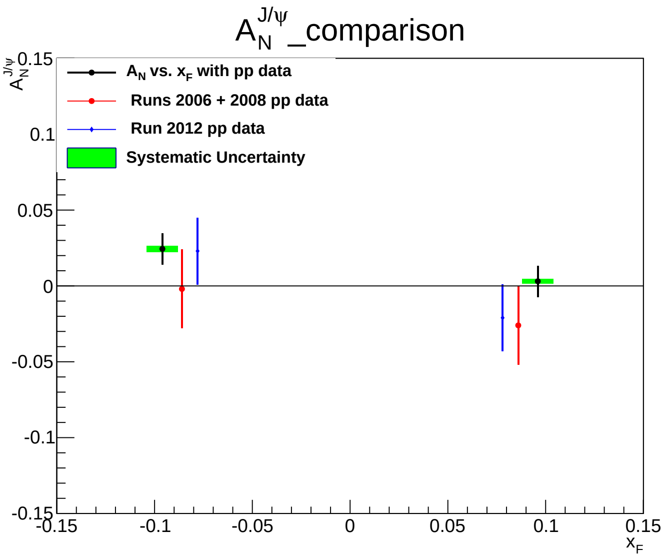

Figure 80: $A_N^{J/\psi}$ in all x_F comparison with previous result with pp data. The fluctuation for each data point is around 1-sigma.